ELSEVIER

Coastal Engineering 47 (2002) 179–210

Coastal Engineering
An International Journal for Coastal, Harbour and Offshore Engineers

www.elsevier.com/locate/coastaleng

Gradation effects in sediment transport

R.J. de Meijer[a,*], J. Bosboom[b,c], B. Cloin[b,c], I. Katopodi[d], N. Kitou[d], R.L. Koomans[a,e], F. Manso[a,f]

[a] *Nuclear Geophysics Division, Kernfysisch Versneller Instituut, Rijksuniversiteit Groningen, 9747 AA Groningen, The Netherlands*
[b] *WL/Delft Hydraulics, Postbus 177, 2600 MH Delft, The Netherlands*
[c] *Netherlands Centre for Coastal Research (NCK), Department of Civil Engineering and Geosciences, Delft University of Technology, Delft, The Netherlands*
[d] *Democritus University of Thrace, Department of Civil Engineering, 67100 Xanthi, Greece*
[e] *Medusa Explorations B.V., Postbus 623, 9700 AP Groningen, The Netherlands*
[f] *Departamento do Geociencas Marinas y Ordenación del Territorio, University of Vigo, Apartado. 847, 36200 Vigo (Pontevedra), Spain*

Abstract

To determine the effects of grain size and density gradation in oscillatory sheet-flow, experiments are conducted in an oscillating water tunnel. A formal derivation of a schematised transport model shows that the transport rates per sediment fraction can be determined with and without the assumption of an active layer. A technique that measures sediment composition from natural occurring radionuclides is used to determine the transport rates without that assumption of an active layer. The measurements on total sediment transport rates and suspended sediment concentrations show that effects of gradation are present. The effects of size gradation are mainly in the increased transport rates of the coarse fraction with respect to the uniform coarse material and the availability at the bed under similar conditions. The experiments on density graded sediments indicate that total mass-transport rates are larger than the mass-transport rates of quartz material, whilst the transport rates of the quartz fraction show that this fraction is not hindered by the availability at the bed.

Keywords: Size gradation; Density gradation; Wave-flume experiments; Sediment transport rates; Bedload; Suspended sediment concentrations; Sediment characterisation; Heavy minerals; Natural radioactivity; Medusa

1. Introduction

Beaches of open seas are good sites to observe effects of selective sediment transport. Beaches show a large variety in morphology from coast to coast and in time at a particular location. At some locations pebble and rock beaches are adjacent to sand beaches and on sand beaches one notices variations in ''sediment'' composition along and across the beach: fine and coarse sand, placers of heavy minerals, concentrations of shells and driftwood and man-made materials such as shoes and bottles.

These observations are the indication that transport processes depend on variations as size, density, shape, sphericity and roundness of grains. Describing transport of a set of spherical grains with one particular diameter is already complicated enough and many models for calculating transport of sediments or of seafloor morphology ignore effects that can occur when sediments with different properties are graded.

* Corresponding author. Fax: +31-503-634003.
E-mail address: demeijer@kvi.nl (R.J. de Meijer).

0378-3839/02/$ - see front matter © 2002 Elsevier Science B.V. All rights reserved.
PII: S0378-3839(02)00125-4

These restrictions were also partly imposed by limitation in computational power. The rapid changes in computer technology and the associated developments of software reduce these limitations and allow incorporation of gradation effects.

Grain size and gradation variations are not only of importance for the "natural" morphodynamic development of the coast but have large implications for the design and effectivity of nourishments as well. The segregation mechanisms underlying the observed cross and along shoreface grain size and density variations are still poorly understood.

Sorting processes occur both in settling and pick up of grains. In settling the fall velocity is dependent on size, shape and density. The settling or fall velocity follows from the equilibrium between gravity and friction acting on the grain. Grains with the same settling velocity are considered to be hydraulic equivalent. Due to the differences in settling velocity, it can be expected that segregation of sediment fractions takes place in the vertical, with the finer fractions suspended at higher elevations. A net onshore transport of coarser and/or denser material relatively close to the bed combined with a net offshore sediment transport of finer and/or lighter material at higher elevations would then result in cross-shore segregation leading to the offshore fining. Pick up of grain was first studied for uni-directional flow (rivers) and has later been extended to oscillatory flow (waves). The effects of sediment density and grain size are different in both processes.

Fig. 1.1 describes the settling velocity and entrainment velocity of sediment grains as function of grain size and density. The settling velocity, w_s, is calculated using the formulation of Cheng (1997); the entrainment velocity is derived from Komar (1987).

The upper figure shows the effect of varying density and grain size on the settling velocity of a sediment particle. For small grain sizes, density variations have little impact on the settling velocity of a grain; for larger grains, the effect of density becomes more important. The lower figure shows the entrainment velocity as a function of density and grain size. Again for small grain sizes, effects of density in the entrainment velocity are small, whilst for larger grain sizes the effect of density dominates. A comparison between both figures shows that effects of to density variations are different in sorting processes due to settling and processes due to entrainment. Whilst grain-size variations will have a larger effect on the settling velocity, variations in density will have larger effects in the entrainment velocity.

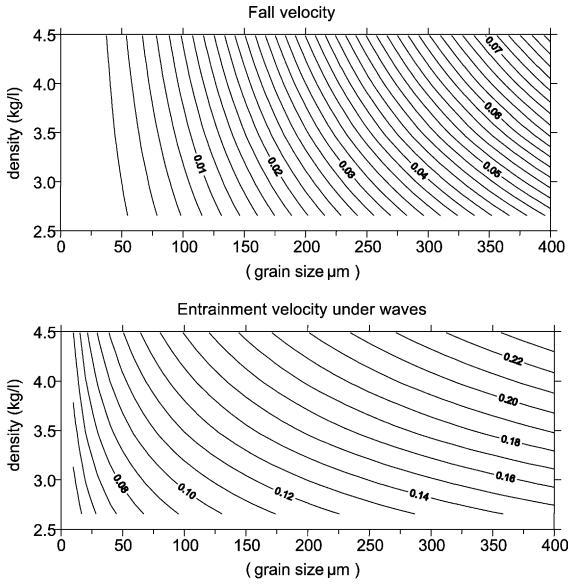

Fig. 1.1. Settling velocities (m s^{-1}) and velocity needed to entrain the sediment as function of grain size and density.

1.1. Field measurements

1.1.1. Size gradation

The effects of size gradation on sediment transport in unidirectional flows were investigated in field measurements (see e.g. Andrews, 1983; Carling, 1983; Hammond et al., 1984; Komar, 1987). All these measurements focus on size sorting of gravel and conclude that in a mixed size (gravel) sediment, the coarser fraction sticks higher into the water and have smaller pivoting angles than under uniform bed conditions. This implies that a mixture leads to a lower entrainment stress for the coarser fraction.

Van Rijn (1997b) gave an overview of field data concerning grain-size variations in coastal sediments reported in literature. Grain-size variations under non-tidal and micro-tidal conditions were studied by Pruszak (1993), Liu and Zarillo (1987), Moutzouris (1988), Boon and Green (1998), Richmond and Sallenger (1984) and Katoh and Yanagishima (1995). Similar studies for meso-tidal conditions were con-

ducted by Migniot and Lorin (1986), Terwindt (1962) and Guillén and Hoekstra (1996). In the framework of the MAST-II programme NOURTEC, grain-size variations were studied extensively along the barrier island of Terschelling on the Netherlands North Sea coast before and after a shoreface nourishment with relatively coarse and well-sorted material. It was found that the grain size is largest near the wave plunge point or in the swash zone from where both an onshore and offshore fining takes place. In the offshore direction the layer of fine material overlying coarser material becomes increasingly thinner. A slight coarsening is observed over the breaker-bar crests, whereas finer material is found in the bar troughs. The adaptation time of the spatial sorting to morphological changes was found to be short, given the fact that the impact of the nourishment with coarser and less well-sorted material had quickly disappeared. Clearly, some dynamic equilibrium of sediment size and hydrodynamic conditions exists. The basic rule appears to be that finer grains are winnowed away from the bed in the most energetic areas by turbulent processes and carried away to less energetic areas.

Gradation effects are also observed for even finer grained materials than sand. At sea and in rivers mud and clay are settling in areas where sand grains have virtually become immobile. In a recent set of measurements the transport of harbour sludges, dredged from Rotterdam harbour, was monitored over a 10×15 km^2 area of the seafloor (Venema and De Meijer, 2001). Using a towable detector system to measure natural radioactivity (see also Section 2.4) and using radiometric fingerprints of sand, silt and clay to derive sediment composition maps, the changes in bottom sediment composition were measured over time. The data clearly showed the large mobility of clays ($d < 16$ μm) being transported in more or less two opposite directions, whereas the silt fraction remained near the dumpsite at about 10-m water depth.

1.1.2. Density

Whereas in transport of gravel, size, sphericity and roundness-gradation effects dominate, grains of beach sands are often almost spherical but consist of mineral grains with quite a range in density (from carbonates < 2 kg/l to cassiterite 7.4 kg/l). von Engelhardt (1937) noticed that on a given place only sand grains with a specific settling velocity are deposited, meaning that the grain-size distribution is a reflection of the hydraulic equivalence (same settling velocity) of the mineral suite. This leads to simultaneous deposition of large grains with lower density and small grains with higher density. von Engelhardt also observed density-dependent sorting in horizontal directions.

Traditionally, minerals and sands are divided in two density fractions according to the separation technique based on the heavy liquid bromoform ($\rho = 2.9$ kg/l). The minerals that float on bromoform (e.g. carbonate, quartz and feldspar) are named light minerals and those that sink are called heavy minerals. Sand deposits with a very high concentration of heavy minerals (>50%) are also named placers.

Selective transport within the suite of heavy minerals has been studied by investigating the heavy mineral composition of sediments collected along beach profiles (see e.g. Koning, 1947; Veenstra and Winkelmolen, 1976; Winkelmolen and Veenstra, 1980; de Moor and de Decker, 1982; Komar and Wang, 1984; Peterson et al., 1985; Meisburger, 1989; Eitner, 1995). The composition is often deduced from counting of heavy-mineral concentrates obtained from sediment samples. In general it is observed that the percentage of total heavy minerals and the relative contribution of the high-density minerals increase in shoreward direction. Komar and Wang (1984) conclude that selective transport must play an important role and that selective transport occurs on all scales: on the beach, during offshore transport and even within ripples. Measurements of Greenfield et al. (1989) and Tánczos (1996) confirm this conclusion and also observed selectivity in onshore transport.

Effects of selective transport are also observed in the longshore direction. Peterson et al. (1985) noticed that placers were best developed along the Oregon coasts (USA) at points of shoreline curvature. At these locations the longshore currents and wave action diminish, resulting in fluid shear-stress gradients. Similarly, concentrations of denser minerals are found near river mouths. This is well known from offshore diamond-mining activities near the Orange River (South Africa) and was studied for the Columbia River (USA) by Li and Komar (1992) and the Nile River (Egypt) by Frihy and Komar (1991, 1993) and Frihy et al. (1995). In the latter study, it was concluded that light minerals are transported from eroding

areas to accretion areas, thereby concentrating the heavy minerals as lags.

1.2. Flume experiments

1.2.1. Effects of size and density

In wave flumes size and density effects in sediment transport were studied by May (1973), Ribberink and Chen (1993), Ribberink and Al Salem (1994), Janssen and Ribberink (1996), Tánczos (1996), Janssen and Van der Hout (1997) and several Japanese groups (see Yeganeh Bakhtiary and Asano, 1998). In their paper, Yeganeh and Asano evaluate experiments under sheet-flow conditions with natural sand ($\rho = 2.65$ kg/l and $d_{50} = 0.2$ mm) of Horikawa et al. (1982), Al-Salem (1993) and Ribberink and Al Salem (1994) and those with artificial materials like imitation pearl, coal dust and plastics with $1.2 < \rho < 1.6$ kg/l and $2.8 < d_{50} < 5$ mm. They try to compare sediment concentration profiles, transport velocity profiles, fluxes and rates by scaling the experiment according to the Shields parameter. For references to the latter experiments, mainly published in Japanese, we refer to Yeganeh Bakhtiary and Asano (1998). The main conclusion of their work is that using artificial particles it is not always possible to reproduce sheet-flow sediment transport even if the Shields number predicts so.

Ribberink and Al Salem (1994) and Ribberink and Chen (1993) conducted experiments in the Large Oscillating Water Tunnel (LOWT) of WL/Delft Hydraulics with second-order Stokes waves using unsieved dune sand ($d_{50} = 0.21$ mm) and fine sand ($d_{50} = 0.13$ mm), respectively. Janssen and Ribberink (1996) and Janssen and Van der Hout (1997) studied the grain-size influence on net-transport rates and sand transport mechanisms. Experiments with fine sand ($d_{50} = 0.13$ mm) were carried out by Janssen in the LOWT. The same flow conditions were used as in the experiments with unsieved dune sand ($d_{50} = 0.21$ mm) (Katopodi et al., 1994). In the above studies, it was found that the grain diameter is an important parameter for the net transport rates. It was found that for the fine sand unsteady effects are very important. The time-dependent sediment concentrations show that the fine sand which is entrained in the positive half wave cycle, does not settle down in that half-wave cycle, but is transported in the succeeding negative half-wave cycle. The net-transport rates were smaller compared to the net-transport rates for dune sand and even became negative for increasing oscillating velocities. The net-transport measurements were used to verify existing quasi-steady and semi-unsteady transport models. It appeared that only for the coarser material the net transport rates can be described in a quasi-steady way.

Janssen and Van der Hout (1997) carried out some experiments to complete the data set for three different grain sizes ($d_{50} = 0.13$, 0.21 and 0.32 mm). Van der Hout (1997) concluded that as long as a condition can be considered as quasi-steady, a smaller grain size results in an increased transport rate.

1.2.2. Effects of size and density gradation

Dibanja and Watanabe (1996) carried out experiments with non-linear waves and a mixture that was composed of fine sand, $d_{50} = 0.2$ mm and coarse sand, $d_{50} = 0.87$ mm. They observed that for mixed sands, sheet flow occurs even at lower velocities than those for uniform sands; likely due to a firmer structure of the sediment bed. Transport-rate measurements showed that armouring of fine sand by the coarse sand gives rise to a significant reduction in the transport rate of the fine sand. The transport rate of the coarse sand was almost unaffected by the presence of the fine sand. Slingerland (1984) classified the effects of sorting of heavy minerals in unidirectional currents according to hydraulic and lift forces and/or shear stress. Slingerland stated that the equivalent entrainment size ratios of heavy to light grains could be four times smaller than would be predicted by settling laws. Tánczos et al. (1995) used two wave flumes in their experiments to study gradation effects under ripple and sheet flow conditions. Under ripple conditions heavy and light minerals were transported in opposite directions and different modes: heavies as bed load and lights in suspension. These effects were also observed by May (1973).

Experiments under sheet-flow conditions were carried out by Tánczos (1996) in the Large Oscillating Water Tunnel (LOWT) of WL/Delft Hydraulics at de Voorst (NL). In these experiments heavy-mineral sand was used taken from a storm deposit of the beach of Ameland. The hydrodynamic conditions were similar as in the experiments of Ribberink and Al Salem (1994) using light-mineral sands. In their experiments,

Tánczos et al. (Tánczos, 1996; Tánczos et al., 1995) observe that:

- both light and heavy minerals are moved in the wave direction;
- only light minerals are collected in the suspension sediment collector.

Tánczos (1996) shows that the transport rates for this sand mixture are considerably lower than for quartz sand and seem to level off with increasing velocity. Based on this levelling off, Tánczos proposes an armouring effect in which the denser grains get concentrated in a thin surface layer and thereby prohibit the lighter grains from being picked up and transported.

1.2.2.1. Effects of porosity. The experiments of Dibanja and Watanabe (1996) showed that for a sediment mixture, the better packing of the bed results in increased adaptation times of the bed forms. Theoretically, the densest system obtainable with spheres is the so-called rhombohedral packing in which a porosity of $\varepsilon = 0.26$ can be achieved (Graton and Fraser, 1935).

In mixtures of larger and smaller grains the smaller grains always interfere with packing of the larger. The greater the range from maximum to minimum particle sizes, the smaller is the porosity of the system. This technique is applied in soil stabilisation and in making concrete and hydraulic and bituminous cements. For a normal distribution of rounded gravel and sand the porosity ε is given as an empirical relation (Winterkorn and Fang, 1975):

$$\varepsilon = 0.385 - 0.08\log\left(\frac{d_{\max}}{d_{\min}}\right) \tag{1.1}$$

in which $d_{\max}$ and $d_{\min}$ are the diameters of the largest and smallest particles, respectively. For the experiments in this paper, a porosity of 0.36 is calculated for the well-sorted sediments, whilst the poor sorted mixture gives a porosity of 0.34.

1.3. Transport and morphological modelling for grain size mixtures

The most straightforward attempts to include the spatial variation of grain size in morphological models make use of the assumption that the sediment sorting adapts quickly to morphological changes, as was observed in the NOURTEC programme. On the basis of these findings a unique relationship was taken into account between water depth and grain size in a cross-shore profile (Roelvink et al., 1995). The usual transport formulas are used to compute the net transport rates using the local median grain size as input. This was found to have a significant influence on the morphodynamic development.

A second step towards taking sediment sorting into account implies the prediction of the behaviour of individual sediment fractions, and hence the spatial sorting effects. Van Rijn (1997a,b) included the effects of size gradation in a cross-shore profile model by considering the individual fractions and the bed-level changes per fraction using a layer model (see below). The total transport rates were computed by dividing the grain-size distribution in a number of sediment fractions each characterised by a certain d_{50} and calculating the transport rates of each fraction separately using the conventional sediment-transport formula for uniform material. In the following, this method is referred to as the size-fraction method. It assumes that the mass-transport rates of a individual fraction, can be computed as the transport rates given by formula for uniform material using the d_{50} of the fraction under consideration, weighted with its percentage of occurrence at the bed. Often the size-fraction method includes a correction in the formula for uniform material which accounts for the differences in exposure to the flow of each fraction in the mixture as compared to a uniform bed composed of that fraction.

These corrections are referred to as hiding and exposure corrections. The size-fraction method has widely been applied (e.g. Egiazaroff, 1965; Ribberink, 1987a,b; and many others). In situations where a model is used which resolves the sediment distribution in the vertical by applying for example a diffusion equation, the size-fraction method implies a bed-boundary condition for the suspended-sediment vertical for each fraction (Deigaard and Fredsoe, 1978; Armanini and Ruol, 1998; Zyserman and Fredsoe, 1991).

An important aspect in situations with graded sediment is the description of the sediment exchange between stream and bottom. In the classical river model of Hirano (1971), the river is schematised by

one ”mixing layer” in the bottom and one “transport layer” in the stream (two-layer model). The two layers interact through the sediment-continuity equation and the bed-material composition is computed. The consideration of the suspended sediment requires in principle a third layer so that the sediments are free to deviate from local equilibrium and their vertical distribution depends on the upstream conditions (three-layer model). Three-layer models were presented by Armanini and Di Silvio (1988) and Rahuel et al. (1989). Moreover, the mixing or exchange layer in the bottom can be divided in two parts: a pavement and a subpavement (four-layer model) (Di Silvio, 1991). Di Silvio and Peviani (1991) compare two- and three-layer models with experimental data and present an evaluation. They find that for slow changes in the hydraulic conditions a two-layer model is sufficient.

The above work on graded-sediment transport is mainly applied to sediment transport and morphological development in rivers. Applications to a coastal environment are still limited. The experiments presented in this paper provide an opportunity to test the validity of the size-fraction method and to investigate the influence of the type of uniform transport formula in applying a size-fraction method.

1.4. Scope

Within the EU programme Marine Science and Technology (MAST III), a project SAFE is funded. Part of the SAFE activity is on gradation effects in sand transport. With support of the EU programme Training and Mobility of Researchers (TMR) section Large Installations Facilities, the LOWT of WL/Delft Hydraulics was used for two series of experiments in 1997. The experimental programme is a continuation of the experiments initiated by Ribberink and Al Salem (1994) and Tánczos et al. (1995) and a follow up on a series of other experiments (Table 1.1).

Tánczos et al. (Tánczos, 1996) used a mixture of minerals with a large range of grain size and densities. The effects that were observed in the experiments may consequently be the result of gradation effects of grain size and density. Thus far it is unknown whether density and grain size effects can be treated independently. But to keep the interpretation of the data as simple as possible one of present experiments was devoted solely to grain size effects and the second one was designed to investigate density gradation only.

The grain size experiment in the LOWT (K-series) used light mineral sands. Experiments were carried out with a mixture of two types of sand with different median grain sizes (d_{50} values). The conditions of the K-series are chosen such that a comparison is possible with previous experiments with uniform sand with $d_{50}=0.13$, 0.21 and 0.32 mm. The sinusoidal wave conditions can be compared with experiments that were conducted by Katopodi et al. (1994), $d_{50}=0.21$ mm; Janssen and Ribberink (1996), $d_{50}=0.13$ mm; and Janssen and Van der Hout (1997), $d_{50}=0.13$ and 0.21 mm. The second-order Stokes wave conditions are similar to the conditions of the experiments by Ribberink and Al Salem (1994), $d_{50}=0.21$ mm and Ribberink and Chen (1993), $d_{50}=0.13$ mm.

In the other experiments (L-series) light and zircon sand have been utilised. The sands have the same d_{50} value, with almost the same grain size distribution but

Table 1.1
Series identifier, median grain size, type of oscillatory sheet flow, net current velocities, root mean square velocity oscillation period and reference for previous experiments conducted in the LOWT

Series	d_{50} (mm)	Type of osc. flow	$\langle u \rangle$ (m s^{-1})	u_{rms} (m s^{-1})	T (s)	Reference
B	0.21	reg + irreg; asym		0.5–0.9	5–12	Al-Salem, 1993
C	0.21	reg; asym + sin		0.6–1.2	6.5–9.1	Al-Salem, 1993
D	0.13	reg; asym		0.5–0.9	6.5	Ribberink and Chen, 1993
E	0.21	reg; sin	0.15–0.4	0.7–1.2	7.2	Katopodi et al., 1994
F	range d_{50}, range ρ	reg; asym		0.5–0.9	6.5	Tánczos, 1996
H	0.13	reg; sin	0.2–0.4	0.65–1.1	4–12	Janssen et al., 1996
I	0.32	reg; sin	0.2–0.4	0.5–1.2	7.2	Janssen and Van der Hout, 1997
J	0.21	reg; sin	0.2–0.4	0.35–0.9	4–12	Janssen and Van der Hout, 1997

reg = regular; irreg = irregular; asym = asymmetric; sin = sinusoidal.

with densities of 2.6 and 4.4 kg/l, respectively. Three combinations of quartz and zircons, 100% zircon, 25% zircon and 7% zircon, respectively, were used in the experiments. The hydrodynamic conditions in the LOWT experiments (L-series) were similar as for the K-series experiments.

The present experiments are the first ones investigating transport of graded sediment under sheet-flow conditions under laboratory conditions. We therefore adapted a similar strategy as proved successful for uniform sediment experiments. Also in the analysis of the data we started from the methodology developed for uniform sediment. In the K-series sediment-composition information on the bed has been obtained by "traditional" sampling; grain size distributions have been derived from a settling tube analysis. In the L-series a settling tube analysis is not straightforward due to differences in density. In the L-series we used a non-invasive, radiometric method and combined it with control measurements using a small size corer. In both series suspended sediment composition is measured by a transverse suction system, whilst concentrations are also measured by optical and conductivity based devices.

Also in the interpretation we adopted the experiences obtained in previous experiments (Tánczos, 1996) in which an active layer of at most a couple of centimetres could be observed, due to the differences in colour between light and heavy minerals. As these layers were quite uniform in colour a homogeneous composition of the layers is assumed.

The main goal of the present set of experiments is to observe deviations from results obtained with corresponding uniform sediment experiments under similar hydrodynamic conditions. At the same time the experiments serve as a test for the measurement strategies for graded sediment experiments. The results supply a database to test, develop and validate descriptions of gradation effects in sediment transport by mathematical models.

This paper reviews the experimental techniques and the data obtained in these two experiments. For details we refer to the data reports (Hamm et al., 1998; Manso et al., 1999). In addition a mathematical layer model is presented, tailored to describe these data.

2. Hydraulic conditions and experimental techniques

2.1. The Large Oscillating Water Tunnel

The Large Oscillating Water Tunnel (LOWT) was designed to simulate water–sediment interaction under waves in the near-shore zone, in the region close to the bottom at a one-to-one scale. Fig. 2.1 presents a schematic view of the LOWT. As can be seen the LOWT has a long rectangular horizontal test section with a cylindrical riser at either end. A piston system in the closed cylinder, driven by a hydraulic servo-cylinder, is capable of simulating near bottom velocities in the test section that correspond to mod-

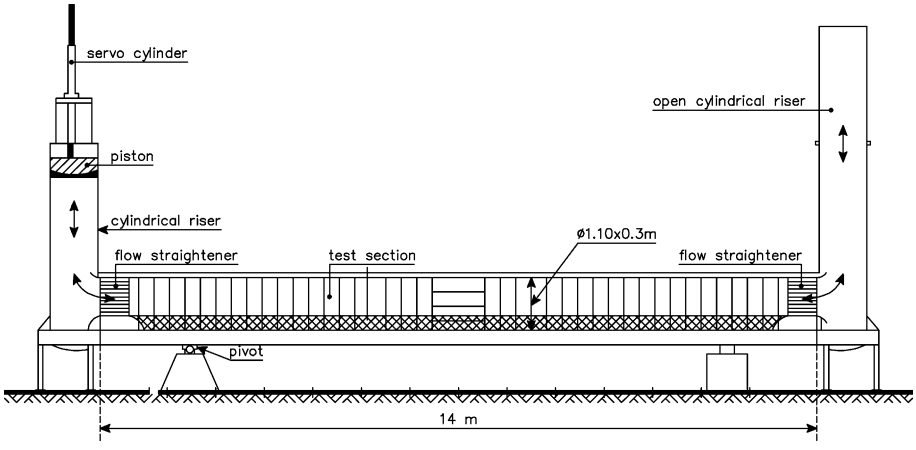

Fig. 2.1. Schematic cross section of the Large Oscillating Water Tunnel at WL/Delft Hydraulics.

erate to rough wave conditions. The steering signal for the hydraulic piston is generated by software. The other riser is open to the atmosphere. Of the test section, that measures approximately $14 \times 0.3 \times 1.1$ m^3, the lower 0.3 m is available for a sand bed and the upper 0.8 m for the oscillatory flow. At both ends of the test section a sand trap is located to collect the sediment that is transported out of the tunnel.

Oscillatory flow can be combined with a current (maximum, 0.5 m/s) via a recirculation flow system connecting the open cylinder with the piston cylinder. This system also contains a sand trap, consisting of a 12-m long, 1.2-m diameter pipe that traps effectively 90% of suspended sediments with a grain size of more than 0.1 mm.

The LOWT is designed to simulate pure horizontal flow. Test measurements indicated that the horizontal velocity amplitude is uniform in the central axis over the middle 10 m of the test section. No systematic variations in the horizontal velocity component in the lower 20 cm of the central 2.0 m were found (Ribberink, 1989).

2.2. Hydraulic conditions and measuring procedures

Part of the experiments were carried out with regular, asymmetric second-order Stokes waves without a current:

$$u(t) = u_1 \cos\omega t + u_2 \cos 2\omega t, \tag{2.1}$$

where $u(t)$ is the near-bed horizontal orbital velocity and ω is the angular frequency of the basic oscillation. The peak velocities under the crest and trough of the wave are given by $u_c = u_1 + u_2$ and $u_t = u_1 - u_2$, respectively. The root-mean square velocity is defined as:

$$u_{rms} = \sqrt{0.5(u_1^2 + u_2^2)} = 0.5\sqrt{u_c^2 + u_t^2}. \tag{2.2}$$

In the K-series experiments in addition to the second-order Stokes wave, a sinusoidal and a saw-tooth wave were applied. The saw-tooth wave is described by:

$$u(t) = u_1(t)\cos\omega t - u_2 \sin 2\omega t. \tag{2.3}$$

"Real" waves propagate in the direction of the crest velocity. In the LOWT the wave direction is equal to the direction of the largest peak velocity.

Table 2.1 lists the hydraulic conditions of the experiments of the K and L series. Each *condition* contains three *runs*. The bed level along the test section was measured before and after each run by a bed-level profiling system. For the K-series the initial situation for all conditions was the same; before every new condition, the upper layer of the sand bed (about 5 cm) was removed from the tunnel and replaced with new, well-mixed sand. Before every run, the erosion hole was filled with new sand and the sediment accumulation at the right-hand (upstream) side of the tunnel was removed. In all conditions sheet-flow conditions were obtained.

2.3. Sand characteristics

In the present experiments four types of sediment were used: quartz sand with a density, $\rho = 2.65$ kg/l

Table 2.1
Wave type, crest and trough velocities in the flume, wave period, net current and sediment compositions in the K and L series experiments

Experiment ID	Wave type	Wave characteristics			Net current, Q (l s_{-1})	Quartz, d_{50} (mm)			Zircon, $d_{50} = 0.21$ mm
		u_c (m s^{-1})	u_t (m s^{-1})	T (s)		0.13	0.20	0.32	
K1	second-order Stokes	1.5	0.8	6.5		0.5		0.5	
K2	second-order Stokes	1.1	0.6	6.5		0.5		0.5	
K3	Sawtooth	1.2	0.7	6.4		0.5		0.5	
K5	Sinusoidal	1.7	1.2	7.2	46	0.5		0.5	
K6	Sinusoidal	1.4	0.5	7.2	89	0.5		0.5	
L1	second-order Stokes	1.3	0.7	6.5					1.0
L2	second-order Stokes	1.8	0.9	6.5					1.0
L3	second-order Stokes	1.3	0.6	6.5			0.93		0.07
L4	second-order Stokes	1.3	0.6	6.5			0.75		0.25
L5	second-order Stokes	1.6	0.8	6.5			0.75		0.25

Table 2.2
Sand properties: grain size and natural radionuclide concentrations

Type	d_{10} (mm)	d_{50} (mm)	d_{90} (mm)	^{40}K (Bq/kg)	^{238}U (Bq/kg)	^{232}Th (Bq/kg)
Quartz (fine)	0.099	0.128	0.182	4.8 (0.5)	5.1 (0.3)	4.87 (0.13)
Quartz (medium)	0.152	0.203	0.279	216 (13)	6.45 (0.07)	6.80 (0.11)
Quartz (coarse)	0.217	0.317	0.457	1.48 (0.17)	1.84 (0.05)	1.76 (0.06)
Quartz (f/c mixture)	0.097	0.194	0.406	3.1 (03)	3.47 (0.15)	3.32 (0.07)
Zircon	0.126	0.201	0.262	ND	2690 (30)	660 (30)

The values in brackets indicate statistical uncertainties (1 STD).
ND, not detectable due to large Th content.

with a median grain diameter, d_{50}, of 0.13, 0.20 and 0.32 mm, and zircon sand with $\rho = 4.6$ kg/l and $d_{50} = 0.21$ mm. In the size-gradation experiment (K-series) a 50%:50% mixture of the $d_{50} = 0.13$ and 0.32 mm quartz sands was used. As can be seen from Table 2.2, the two fractions hardly overlap in grain size and the composition of bed samples can be determined by either sieving or settling. It should be pointed out that the density of the quartz sand was estimated and hence was assumed to be independent of grain size.

Fig. 2.2 shows the grain-size distribution and the cumulative weight percentage of the $d_{50} = 0.13$ and 0.32 mm sands together with the data for the 50%:50% mixture resulting in a $d_{50} = 0.21$ mm. The figure confirms the small overlap in grain size of the two initial fractions and shows the somewhat shouldered distribution of the mixture. As follows from Table 2.2, the activity concentrations of the natural radionuclides U and Th in the coarse and fine quartz sand differ enough to measure the mixture composition radiometrically (see Eq. (2.5)). This method was only tested for samples of the sand trap after the experiments.

In the density gradation experiment (L-series) mixtures of quartz and zircon sand were used. Both fractions have a $d_{50} = 0.20$ mm. The measured average densities are 2.66 ± 0.02 kg/l for quartz sand and 4.61 ± 0.04 kg/l for zircon sand. Fig. 2.3 shows the grain-size distribution and the cumulative weight percentages for the two sands. One notices that the distributions for the two sands are quite similar and can be considered identical for analytical purposes. For the same token the densities are assumed to be independent of grain size. As follows from Table 2.2

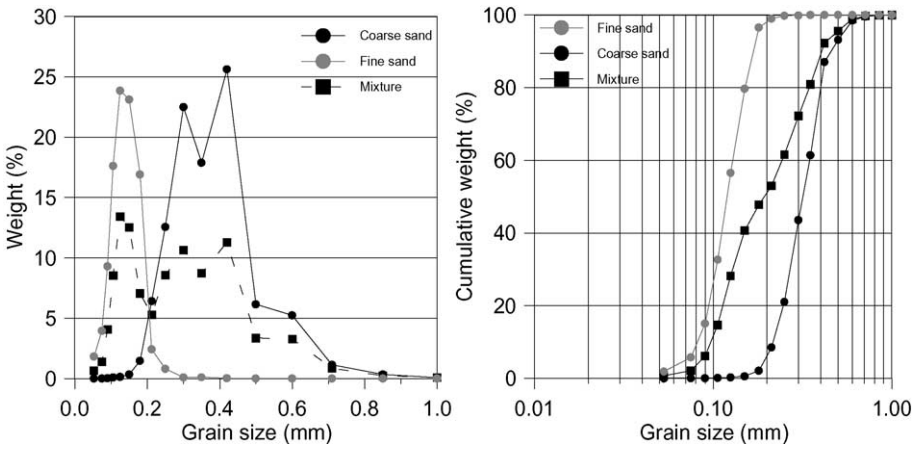

Fig. 2.2. Grain size distribution and cumulative weight percentage for fine and coarse quartz sand used in the size-gradation experiments and the calculated values for a 50%:50% mixture of the two.

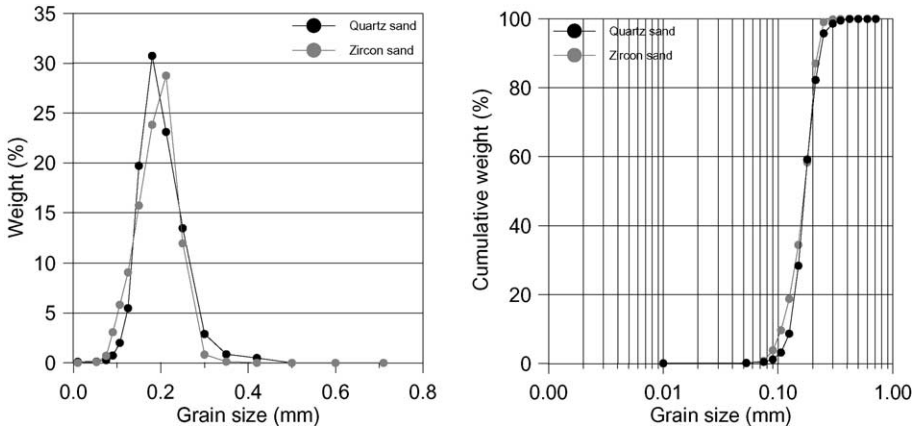

Fig. 2.3. Grain size distributions and cumulative weight percentage for medium quartz and zircon sand used in the density-gradation experiments.

there is a very large difference in the U and Th concentrations between the quartz and the zircon sands.

Activity concentrations in sand samples were measured with a hyper-pure Germanium (HPGe) γ-ray detector. The detector has a high-energy resolution for γ-rays with energies between 0.12 and 3 MeV. To suppress ambient radiation the detector is placed inside a 10-cm thick "old" lead shielding. The activities are determined from the content of peaks in the γ-ray spectrum according to standard procedures (Dutch Norm NEN 5623), more extensively described in de Meijer (1998).

2.4. Measuring techniques

2.4.1. Velocity

The LOWT is equipped with a forward-scatter laser-Doppler system. With this system at every desired position in the test section of the tunnel the horizontal velocity component can be measured. The method is based on the Doppler shift of incident laser light due to moving particles in the water. It determines water velocities with an accuracy of 1.7%. In the present experiments, the laser-Doppler system was positioned in the middle of the test section, at 40 cm above the bottom of the flume (corresponding to about 10 cm above the sediment bed).

The Acoustic Doppler Velocity meter (ADV) measures three components of the velocity in a certain volume. The measuring probe consists of four ultrasonic transducers: one transmission transducer at the bottom of the stem and three receiving transducers pointing at the sampling volume. The receiver transducers measure the velocity by the Doppler shift in the signal scattered by the moving particles.

2.4.2. Concentration

To measure sediment concentrations, three different systems are used: optical concentration meter (OpCon), the Conductivity Concentration Meter (CCM) and a transverse suction system.

The OpCon measures sand (volume) concentrations by the intensity reduction of infra red light. The sensitivity of the instrument allows the measurement of concentrations in the range of 0.005–2 vol.%; the height of its sensing volume is 2.6 mm. The CCM is an instrument to measure large sand concentrations (5–50 vol.%) with a four-point electro-resistance method. A constant AC current is maintained between the two outer electrodes and the voltage between the two inner electrodes is measured. The conductivity will decrease with increasing sand concentrations. According to Ribberink and Al Salem (1992) the height of the sensing volume is approximately 1 mm.

A transverse suction system, as developed by Bosman et al. (1987), was mounted in the test section to measure time-averaged suspended sediment concentration profiles $C(z)$ (Bosman et al., 1987). It was located in the middle of the LOWT at $y = 0.15$ m and $x = 2.3$ m with the 10 nozzles (∅ 3 mm) perpendicular to the (horizontal) fluid motion. The fluid with the sus-

pended sediment was pumped out of the LOWT with a constant velocity and collected in reservoirs. In a volume meter the wet volume of the sand present in the reservoirs was determined from which the suspended-sediment concentrations (g/l) in the suction samples were calculated assuming a certain porosity. The ratio between the concentration in the suction samples C_s and the actual sediment concentration in the flow C_c is given by the trapping efficiency $\alpha = C_s/C_c$. This factor depends amongst others on the grain size and is constant if the suction velocity is high enough (≈ three times the fluid velocity). Its value was determined in a calibration procedure for several types of sediment Bosman et al. (1987).

2.4.3. Bed height

The bed level was measured with a profiling system positioned on a carriage. The system contains three profilers based on conductivity measurements, two at 0.05 m from the sidewall and one in the centre. The bed level is defined as the average of the three readings. A profiler measures the conductivity in a sampling area and by maintaining a constant value the tip of the profiler remains at a constant distance from the sediment bed.

2.4.4. Sediment samples

Samples of the sediment bed were taken into two ways. In the K-series a perspex cylinder 0.1 m height and 0.1 mm diameter was placed into the sediment for about 0.05 m. Subsequently the top layer of sediment was siphoned into buckets. For the net transport measurements samples of 4–5 mm height were taken at five locations along the tunnel. To determine the grain-size distribution as function of depth, subsequently five samples of 2 mm were collected. The grain-size distribution of each sample was determined with a settling tube.

In the L-series a syringe system was used for sampling. A ∅ 2.5 cm syringe with its narrow part removed was pressed into the sediment bed. While keeping the piston fixed the syringe is pulled back. The collected sediment could be pressed out and subsamples of the desired thickness were collected.

2.4.5. In situ sediment composition

The sediments used in the L-series consisted of quartz and zircons with a similar size distribution and a distinctly different average density. In addition the two sediment compounds differ several orders of magnitude in their uranium (^{238}U) and thorium (^{232}Th) contents. This allows a determination of the sediment composition both in-situ and in the laboratory. For a sediment containing a mass fraction μ_z of zircons and hence $(1-\mu_z)$ of quartz, the activity concentration, A, of either radionuclide is given as:

$$A = \mu_z A_z + (1-\mu_z)A_q \tag{2.4}$$

or

$$\mu_z = \frac{A - A_q}{A_z - A_q}. \tag{2.5}$$

In these expressions A_z and A_q are the activity concentrations in the pure zircon and quartz, respectively.

In the flume, the activity concentrations for radionuclides of the uranium and thorium decay series were determined using the MEDUSA system of the KVI (de Meijer, 1998). This system consists of a 15-cm long, 5-cm diameter scintillation crystal for γ-ray detection and associated hard and software for spectrum analysis and stabilisation. The system measures the activity concentration of the sediment in a few seconds.

For the application in the LOWT, the detector was mounted in a lead collimator to shield it from room background. It was placed in a carriage that similar to the bed-profiling system could be placed on a rail on the flume after the flume was opened. The height of the detector was adjusted such that the detector remained at least a few centimetres above the bed. A schematic view of the detector is presented in Fig. 2.4.

For these experiments, the MEDUSA system is calibrated for absorption of γ-rays by the water between detector and sediment bed and for the solid angle in this geometry. A series of calibration measurements were carried out in the LOWT above sediment bed containing 7% zircon (by mass) (Manso et al., 1999). The total activity concentration of the nuclides ^{238}U and ^{232}Th is the result of γ-rays that are emitted from the total 30 cm of sediment. However, due to self-absorption of γ-rays in the sediment, part of these γ-rays are absorbed. The total flux of γ-rays on the sediment surface can therefore be described as coming

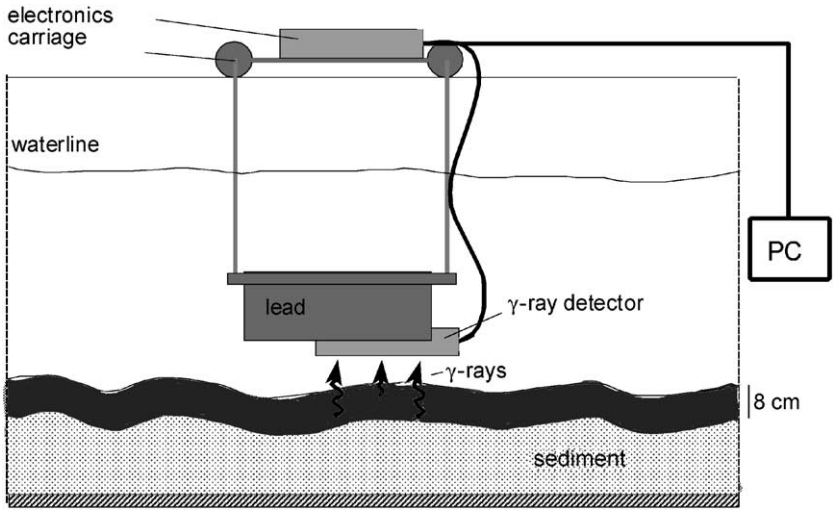

Fig. 2.4. Schematic presentation of the MEDUSA detector set up used in the present experiments (L-series).

from an effective layer of sediment without self-absorption. Measurements of sediment properties (Koomans et al., 1999, Koomans, 2000) indicate that this thickness is ~ 8 cm for quartz. Therefore, the average zircon concentration is measured for the upper 8 cm of the sediment and used in the determination of the sediment transport rates. The results of Manso et al. (1999) are corrected for this estimation. Moreover, uncertainties presented in the data report of Manso et al. (1999) are adjusted by using an error propagation that accounts for uncertainties in activity concentrations rather than of density.

The reason for this change is that in the work of Manso et al. (1999) the densities are derived from activities concentrations. In the relation between density and activity concentrations, the latter ones occur as well in the nominator and the denominator. By using "standard" error propagation (in which all quantities are considered to be independent) the uncertainty in the resulting densities is unrealistic large. Therefore in this work all operations are made in activity concentrations, which only in the last step are converted to densities (Koomans, 2000).

2.4.6. Zircon concentrations sediment samples

The concentrations of zircon in sand mixtures were determined radiometrically using Eq. (2.5) and taking the activity concentrations of $^{238}U + ^{232}Th$ and gravimetrically by weighing samples dried and underwater. The weighing procedure leads to the specific density of the sample ρ:

$$\rho = \frac{m_d \rho_w}{m_d - m_u}, \tag{2.6}$$

where ρ_w is the specific density of water and m_d and m_u are the dry and underwater mass of the sample.

Similar to Eq. (2.5) one can derive that:

$$\mu_z = \frac{\rho_z}{\rho} \frac{\rho - \rho_q}{\rho_z - \rho_q}, \tag{2.7}$$

with ρ_q and ρ_z being the specific densities of the quartz and zircon sands, respectively.

3. Mathematical formulation

This section gives a brief description of the mathematical formulations and concepts of graded sediment transport. First, the bed schematization and the consequent formulation of the bed material are described, the simplified equations that have been used in the two experiments (series-K grain-size gradation, series-L density gradation) are given and the approaches followed in the experiments are discussed. A detailed derivation of the equations from conservation principles, the simplifying steps followed and the approximate expressions used in the experiments can be found in Kitou and Katopodi (1999).

3.1. General

3.1.1. Sediment grain size and density gradation

Sediment non-uniformity is generally treated by considering a number of discrete grain classes with a representative grain size or density of the solid matter. In principle the bed composition can be described either by the fractional contributions of each grain class β_j to the volume of solid matter or by their fractional contributions μ_j to the mass of solids in a bed sample. Since mass and volume are related trough the definition of density the two fractional descriptions are equivalent, and become identical for sediments of constant density. In the following the mass related description μ_j will be used:

$$\mu_j = \frac{m_j}{m} \tag{3.1}$$

with

$$\sum_{j=1}^{J} m_j = m \tag{3.2}$$

where μ_j (−) is fraction of the jth grain class by mass; m_j (kg) is mass of solids of the jth grain class; m (kg) is total mass of solids.

Then it follows that the sum of all fractions is unity.

$$\sum_{j=1}^{J} \mu_j = 1 \tag{3.3}$$

Moreover an equation that relates the mean density of solids and the mass contributions of all grain classes can be derived.

$$\frac{1}{\rho} = \sum_{j=1}^{J} \frac{\mu_j}{\rho_j} \tag{3.4}$$

where ρ_j (kg/m^3) is density of solids of the jth grain class; ρ (kg/m^3) is mean density of solids.

3.1.2. Schematization

The description of the sediment transport processes with graded sediments is more complicated than with uniform sediments because the transport depends on the composition of the upper layer of the bed but also alters the composition itself.

For the mathematical representation of sediment exchange the physical domain is divided into three layers plus the underlying material layer (see Fig. 3.1):

- The suspended load or stream layer: this is the upper layer where sediments are conveyed in

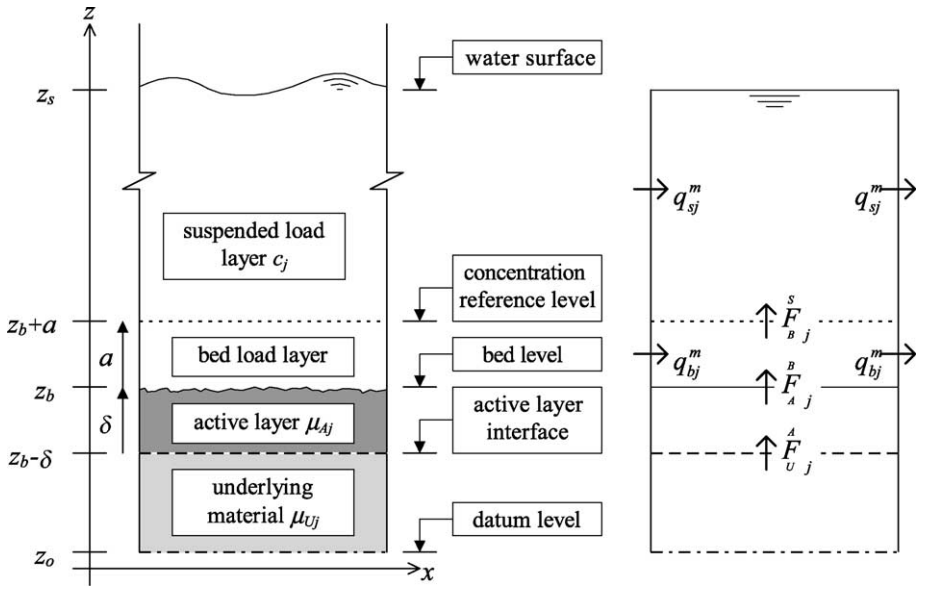

Fig. 3.1. Physical domain and schematic control volumes.

suspension and are described in terms of concentration.
- The bed load or bottom layer: this is a thin layer above the bottom surface where sediments are transported as bed load by sliding, rolling and saltations.
- The active bed or mixing layer: this is a thin layer below the bottom surface where only vertical exchange of sediments takes place. The grains are assumed to be always uniformly mixed in the vertical whilst their composition varies in time and in the horizontal.
- The underlying or undisturbed material layer: this is a semi-infinite layer where the sediments keep the original bed composition.

The two upper layers, where sediment transportation takes place, are sometimes termed as "the transport layers" whilst the two lower ones are called "the bed layers".

In the figure the conceptual sediment fluxes during the transport process are also shown:

c_j	kg m^{-3}	mass concentration of the jth grain class
q_{sj}^{m}	kg/s m^{-1}	suspended-load transport of the jth grain fraction by mass
q_{bj}^{m}	kg/s m^{-1}	bed-load transport of the jth grain class by mass
q_j^m	kg/s m^{-1}	$q_j^m = q_{sj}^m + q_{bj}^m$ transport of the jth grain class, by mass in the transport layers
F_{Bj}^{S}	kg/s m^{-2}	sediment flux of the jth grain class by mass between bed-load and suspended layer
F_{Aj}^{B}	kg/s m^{-2}	sediment flux of the jth grain class by mass between active and bed-load layer
F_{Uj}^{A}	kg/s m^{-2}	sediment flux of the jth grain class by mass between underlying and active layer

3.1.3. Formulation of the bed material

The bed layers (active and underlying layer) consist of sediment grains that are in contact with each other during the transport processes. Thus the fraction of the bed bulk volume occupied by solid matter equals $(1-\varepsilon)$, where ε denotes the porosity. Consequently the dry density of the sample equals $\rho(1-\varepsilon)$, where ρ is the mean density of solids. The composition of the bed material is described by the fractional contributions μ_j of each grain class to the mass of solid matter in a bed sample. It follows that the contribution of the jth grain class to the dry density equals $\rho\mu_j(1-\varepsilon)$.

The active layer is actually the reservoir of sediments from which grains can be actively entrained and transported. The thickness of this layer δ is related locally to the grain characteristics of the sediment mixture (i.e. the grain composition) or to the ripple height in the case of bed forms.

The two-layer schematization of the bed implies a particular structure of the grain fractions μ_j as functions of space and time (Eq. (3.5)). The active layer is assumed to be well mixed by the transport process, so that the grain fractions μ_{Aj} within the active layer have no vertical structure. Since μ_{Aj} interact with the transport process itself, it can give horizontal and temporal variations. Below the active layer there is the underlying layer, with grain fractions μ_{Uj}. Its composition may vary arbitrarily in all spatial directions, but cannot change directly in time because it is not directly subject to movement. Material can be exchanged between the active layer and the underlying layer through their interface. This exchange is due to time variations of the active-layer interface level during sedimentation or erosion, as will be outlined later on. This leads to a function structure:

$$\mu_j(x,z,t) = \mu_{Aj}(x,t) : z_b > z > z_b - \delta,$$
$$\mu_{Uj}(x,z) : z_b - \delta > z \qquad (3.5)$$

where μ_j (−) is fraction of the jth grain class by mass (percentage); μ_{Aj} (−) is fraction of the jth grain class by mass (percentage) in the active layer; μ_{Uj} (−) is fraction of the jth grain class by mass (percentage) in the underlying layer.

Bed porosity depends, in general, on the geometric characteristics of the grains (size and shape) and on the fractional participation of each grain class. The common approach in the literature is to consider porosity as independent of the bed composition. Nevertheless, under the assumption of a known dependence of porosity on the grain fractions, it can vary also in time and space in a similar manner to the grain fractions themselves.

In the case of density gradation, the mean density of solids in a bed sample ρ depends on the fractional

participation of the grain classes. This implies a similar structure, as function of space and time, to the grain fraction themselves.

3.2. Simplified formulations for grain size (series-K) and density gradation (series-L)

In transport experiments, estimations of transport rates at any location of the flume are based on measurements of sand displacement during the experimental run. The measurements for a particular location are based on conservation statements of mass. The computations lead to time mean values of transport over the duration of the experiments that are supposed to be estimations of slowly varying (quasi-steady) wave-averaged values.

For uniform sediments it is common to measure differences of the bulk volume including pores, or in other words changes of the bed level. With graded sediments one has to estimate the sand displacement separately for each class of grains. Measurements of the sand displacement along the flume section can be carried out in different ways depending on the procedure employed.

For the K and L series, the determination of the sediment composition of the bed was approached differently. In the K-series (uniform density and size gradation) the grain-size compositions are based on samples from the upper (active) layer of the sediment bed. For the L-series (uniform grain size and density gradation) the averaged density of the entire bed column is derived from the radiometric properties of the sediment. Therefore, two different approaches in the formulation of the transport rates are used.

3.2.1. Series-K

In the K-series experiments a sand mixture with bimodal *size gradation* was used. The sand consists of two grain classes ($J=2$) with different sizes (fine and coarse) and with the same density of solid matter. Measurements are based on sediment-balance statements *by volume*. A conservation statement that incorporates the layered schematization can be derived for each class of grains. For constant density this statement reduces to a volume-balance equation and can be simplified further by assuming constant porosity ε_o and by neglecting time variations of the active layer thickness δ and of the storage term in the suspended-load layer. The simplified equation reads:

$$(1-\varepsilon_o)\delta\frac{\partial \mu_{Aj}}{\partial t}+\mu_j^*(1-\varepsilon_o)\frac{\partial z_b}{\partial t}=-\frac{\partial q_j^v}{\partial_x} \tag{3.6}$$

where q_j^v ($m^3/s\ m^{-1}$) is transport of the jth grain class by volume in the transport layers.

The bed-composition parameter μ_j^* is associated with sediment exchange at the active-layer interface and is specifically related with time variations of this level. In the case of a time decreasing interface level (erosion), underlying material is incorporated into the active-layer as this level drops. In the case of a time increasing interface level (deposition), active layer material is transferred to the underling layer.

$$\mu_j^*=\mu_{Aj}:\left(\frac{\partial z_b}{\partial t}-\frac{\partial \delta}{\partial t}\right)\geq 0,$$

$$\mu_{Uj}:\left(\frac{\partial z_b}{\partial t}-\frac{\partial \delta}{\partial t}\right)<0 \tag{3.7}$$

It can be shown that the corresponding equation of total sediment balance, derived by summation from the grain class specific equations, reads:

$$(1-\varepsilon_o)\frac{\partial z_b}{\partial t}=-\frac{\partial q^v}{\partial x} \tag{3.8}$$

with

$$q^v=\sum_{j=1}^{J}q_j^v \tag{3.9}$$

where q^v ($m^3/s\ m^{-1}$) total transport of all grain classes by volume in the transport layers.

The formulations used for the transport computations in the experiment are derived from the above equations by integration. The procedure provides estimations of the transport rates per grain class q_j^v and of the total transport rate q^v along the flume as well as the constant values for porosity ε_o and active layer thickness δ. The technique is based on measurements of the active-layer composition, bed profiles and volumes of solids in the sand traps per grain class.

3.2.2. Series-L

In the L-series experiments a sand mixture uniform in size but with *density gradation* was used. The sand consists of two grain classes ($J=2$) with different density of solids (light–heavy) but with the same size

of grains. Measurements are based on sediment-balance statements *by mass*. A sediment-balance equation can be written, for each grain class, concerning mass of solids below the bed surface. In its general form it refers to a control volume (column) extended from an arbitrary datum level z_o up to the bed surface z_b. This equation can be simplified by assuming constant porosity ε_o and neglecting time variations of the storage term in the suspended-load layer. Furthermore by considering the channel floor as the datum level z_o and by introducing the averaged value of the grain-class contribution $\rho\mu_j$ to the density of solids ρ over the entire column of the bed material, this equation reads:

$$(1-\varepsilon_o)\frac{\partial}{\partial t}(\overline{\rho\mu_j}(z_b-z_o)) = -\frac{\partial q_j^m}{\partial x} \tag{3.10}$$

with

$$\overline{\rho\mu_j} = \frac{1}{z_b-z_o}\int_{z_o}^{z_b}\rho\mu_j \mathrm{d}z \tag{3.11}$$

where q_j^m (kg/s m^{-1}) in the transport of the jth grain class by mass in the transport layers.

It can be shown that the corresponding equation of total sediment balance, derived by summation from the grain class specific equations, reads:

$$(1-\varepsilon_o)\frac{\partial}{\partial t}(\bar{\rho}(z_b-z_o)) = -\frac{\partial q^m}{\partial x} \tag{3.12}$$

with

$$\bar{\rho} = \frac{1}{z_b-z_o}\int_{z_o}^{z_b}\rho \mathrm{d}z \tag{3.13}$$

$$q^m = \sum_{j=1}^{J} q_j^m \tag{3.14}$$

where q^m (kg/s m^{-1}) is the total transport of all grain classes by mass in the transport layers.

The formulations used for the transport computations in the experiment are derived from the above equations by integration. The procedure provides estimations of the transport rates per grain class q_j^m and of the total transport rate q^m along the flume. The computations are based on measurements of the averaged density of the entire bed column (via radiometry), bed profiles and masses of solids in the sand traps per grain class.

The averaged density values of solids over the entire column of the bed material can be described by:

$$\overline{\rho\mu_1} = \rho_1\frac{\bar{\rho}-\rho_2}{\rho_1-\rho_2}$$

$$\overline{\rho\mu_2} = \rho_2\frac{\bar{\rho}-\rho_1}{\rho_2-\rho_1} \tag{3.15}$$

The above means that the averaged values of the grain class components $\overline{\rho\mu_j}$ over the entire column of the bed material can be computed from averaged values of density of solids ρ. Eq. (3.15) shows the depth-averaged form of the sediment composition measured with the MEDUSA system (see Eqs. (2.5) and (2.7)).

3.3. Discussion on the formulations used in the measurements

The two series of experiments had a different nature of the sediment mixtures. As a result different measuring techniques and formulations have been used.

In the K-series experiments two grain-size classes were used (fine–coarse). The calculations of sediment transport are based on measurements of the active-layer composition, bed profiles and volumes of solids in the sand traps. In the L-series experiments two grain-density classes were used (light–heavy) and the calculations of sediment transport are based on in situ measurements of the density of solids averaged over the bed column (via radiometry), the bed profile and mass of solids in the sand traps.

For both experiments constant porosity was assumed. This is not accurate for sediment mixtures with different grain sizes (series-K) but the assumption is justified for sediments uniform in size (series-L). The major difference is that for series-K a modeling schematization (active layer) was involved while for series-L the formulation was fundamental.

Even though in the previously presented formulations the time evolution of sediment suspension was neglected (storage term) in fact it is present in the experimental results. This is because the computation is based on the differences of the bed before (no suspension) and after the experiment (concentration has settled). However, attention is needed in analysing (small) sediment samples of the bed surface at the end

of the experiment because they contain material that was in suspension during the transport process.

In the series-K experiment an active layer was assumed, which added inaccuracies to the measurements. An alternative procedure could be to extract entire columns (cores) of bed material for a direct and more accurate evaluation of the amount of solids per class $\rho\mu_f(1-\varepsilon_o)$.

4. Results

4.1. Total transport rates

4.1.1. Size gradation

Net specific sediment-transport rates (excluding pores) were inferred from change in profile using the volume balance Eq. (3.8) with a constant porosity value $\varepsilon=0.4$, based on previous experiments. Per run, a right-and left-hand estimate of the sediment-transport rate in the middle of the section can be made (see Section 3.2.1). The average value of the two estimates is taken as the total transport rate for the respective runs. The two estimates differ only slightly except for the first run of each condition, which is most likely related to the fact that before every new condition, the upper layer of the sand bed (about 5 cm) was removed from the tunnel and replaced with new, well mixed sand. The compaction of this new layer during the first run of a new condition results in a porosity value deviating from the assumed value $\varepsilon=0.4$. Note that none of the below given transport rates are corrected for side-wall effects, as explained by Dohmen-Janssen (1999).

Each condition involved three runs and hence the net sediment-transport rates per condition are based on three transport estimates. In Table 4.1, the net sediment-transport rates averaged over all runs of each condition are presented. The second column in Table 4.1 shows the standard deviation σ.

Table 4.1
Net sediment-transport rates and standard deviations for the various conditions of the K-series

Run	$\langle q_{avg}\rangle$ (10^{-6} m^2 s^{-1})	σ (10^{-6} m^2 s^{-1})
K1	35	4
K2	17	0.3
K3	18	2
K5	79	11
K6	73	6

The results in Table 4.1 show that the transport rates in the conditions K2 and K3 are lower, are medium in K1, and are higher in K5 and K6. The results will be further discussed in Section 5.

Van der Wal (1996), Van der Hout (1997) and Cloin (1998) made a detailed study on the accuracy of the transport rates in the wave tunnel inferred from profile deformation. It was found that the major contributions to inaccuracies in the transport rates result from uncertainties in: (1) bed porosity (and the assumption of time and location independent porosity); (2) total eroded volume in the tunnel as determined from three parallel bed profiles measured by the bed-level sounding system; and (3) total weight of sand in the sand traps (related to a loss of sands in the traps). Based on these studies, the uncertainties in the net sediment-transport rates related to these three factors are estimated to amount to a maximum of respectively 20%, 10% and 10% at most.

Fig. 4.1 presents the transport rates as function of the third-power velocity moment. In this figure, the K5 and K6 results are compared to the values for uniform grain-size experiments. Most transport formulae assume a linear relationship between the transport rate and a third or higher power of the velocity moment, which seems to be the case for the results in Fig. 4.1. The only significant dependence on the mean velocity is observed for the fine sand ($d_{50}=0.13$ mm). The slower increasing transport rates for smaller mean velocities are related to time-lag effects between wave orbital velocity and concentrations within the wave cycle. Comparing the results for K5 and K6 we see that the transport rate of K5 corresponds both to the transport rates of the $d_{50}=0.21$ and 0.32 mm experiments, but deviates from the corresponding $d_{50}=0.13$ mm. For K6, the transport rate corresponds to the $d_{50}=0.13$ and 0.21 mm values, but differ from the $d_{50}=0.32$ mm values. From this comparison one may conclude that in the K5 condition the mixture acts more as the medium and coarser fractions whereas in K6, the mixture acts more as the fine fraction.

For the second-order Stokes conditions (K1 and K2), a comparison of transport rates is shown in Fig. 4.2. Also this figure shows that the uniform fine material (D-series) exhibits phase-lag effects (Doh-

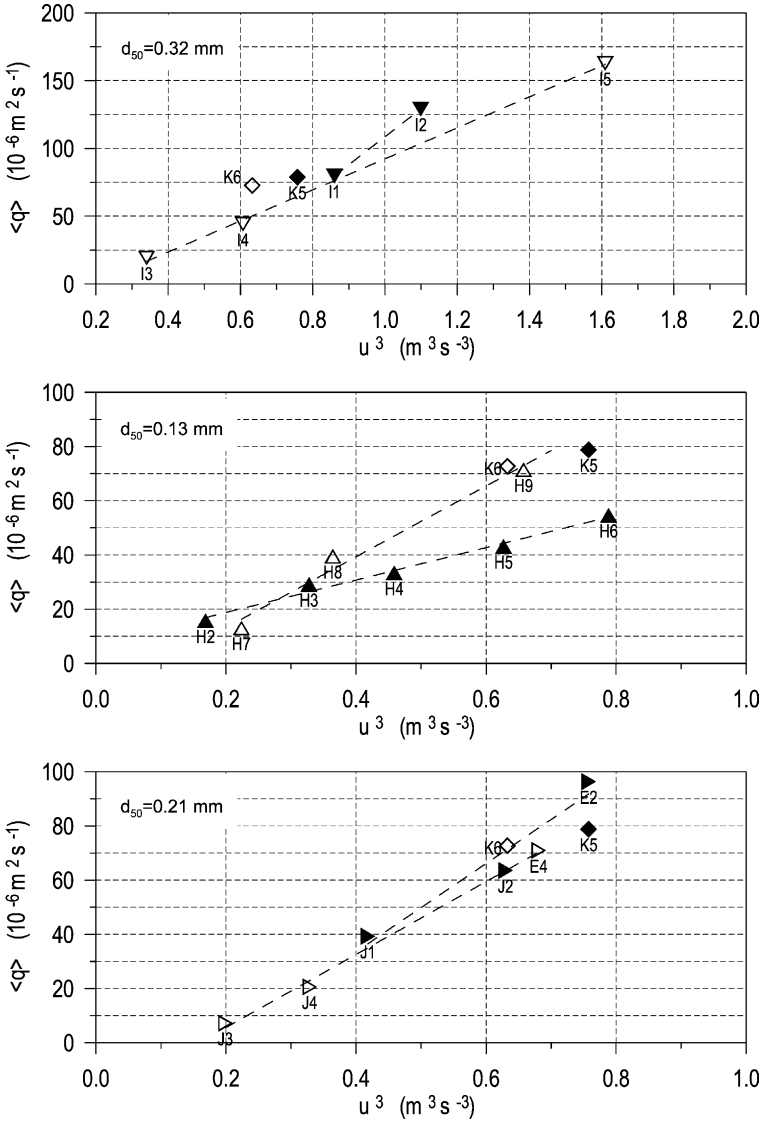

Fig. 4.1. Total net-transport rates in the middle of the flume for sinusoidal waves plus current for uniform sand with $d_{50}=0.32$ mm (upper plot), $d_{50}=0.13$ mm (centre) and $d_{50}=0.21$ mm (lower plot) as a function of the third power velocity moment $\langle |u|^3 \rangle$ (m^3/s^3). Open and closed symbols refer to a mean velocity of 0.4 and 0.2 m s^{-1}, respectively. The letters refer to previous LOWT experiments (see Table 1.1). Total net-transport rates for the mixture of K6 and K5 are shown in every plot.

men-Janssen, 1999) for increasing velocity moment the net-transport rates decrease and eventually even reverse sign (see e.g. K1 and D12). This effect can be understood from phase difference between wave orbital velocity and sediment concentration. Unfortunately, no data are available for the coarse uniform sediment.

4.1.2. Density gradation

4.1.2.1. Profile and development of sediment composition. Profiles were measured at the beginning and at the end of each run. The initial condition for each run was the same: the sediment was homogeneously mixed, placed in the flume and the bed was flattened.

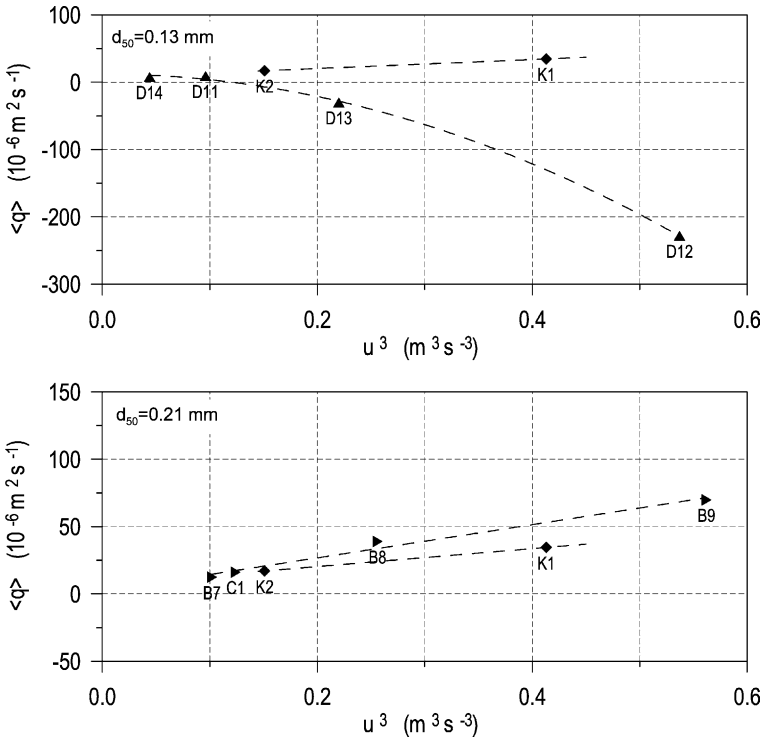

Fig. 4.2. Total net-transport rates in the middle of the flume for second-order Stokes waves without a current for uniform sand with $d_{50}=0.13$ mm (upper plot) and $d_{50}=0.21$ mm (lower plot) as a function of the third power velocity moment $\langle |u|^3 \rangle$ (m^3/s^3). The letters refer to the various LOWT experiments (see Table 1.1).

The profile development during the runs was similar for all conditions: at the beginning an erosion hole develops at the left-hand side of the flume, whereas sediment accumulates at the right-hand side. In the conditions L1 and L2, with 100% zircon sand, large-scale ripple structures developed throughout the flume and even at the highest possible velocity ($u_{rms}=1.0$ m s^{-1}) sheet-flow conditions could not be achieved. At the other conditions only minor oscillations in the bed were noticed.

At the end of each run the sand in the traps was collected, dried and weighed. The concentrations of zircon were determined gravimetrically and radiometrically. Table 4.2 presents an overview of the masses, corrected for the sand losses in the traps, and the corresponding zircon concentrations.

From Table 4.2 one notices that the sand trap at the right-hand side, at the down-stream part of the tunnel collects more sand than the trap at the left-hand side. The sand in the right-hand sand trap contains for the runs L3–L5 some zircons, whereas the trap at the left-hand side contains almost pure quartz sand.

Fig. 4.3 presents the profile of the initial and final bed of condition L4 and the zircon concentrations obtained from the syringe samples and of the MEDUSA measurements. In the initial profile, the zircon concentrations obtained from the syringe and MEDUSA measurements are the same. In the final profile the MEDUSA

Table 4.2
Mass and composition of sediment in the sand traps for the five conditions of the L-series

Run	Left-hand side		Right-hand side	
	m (kg)	Zircon (grav) (%)	*m* (kg)	Zircon (grav) (%)
L1	0.2 (0.0)	73 (11)	3.0 (0.1)	86 (11)
L2	4.8 (0.2)	99 (11)	9.8 (0.4)	97 (11)
L3	2.2 (0.2)	1 (6)	7.5 (0.5)	– 7 (6)
L4	2.6 (0.2)	10 (6)	7.2 (0.5)	– 6 (6)
L5	11.6 (0.8)	12 (6)	12.9 (0.9)	– 7 (6)

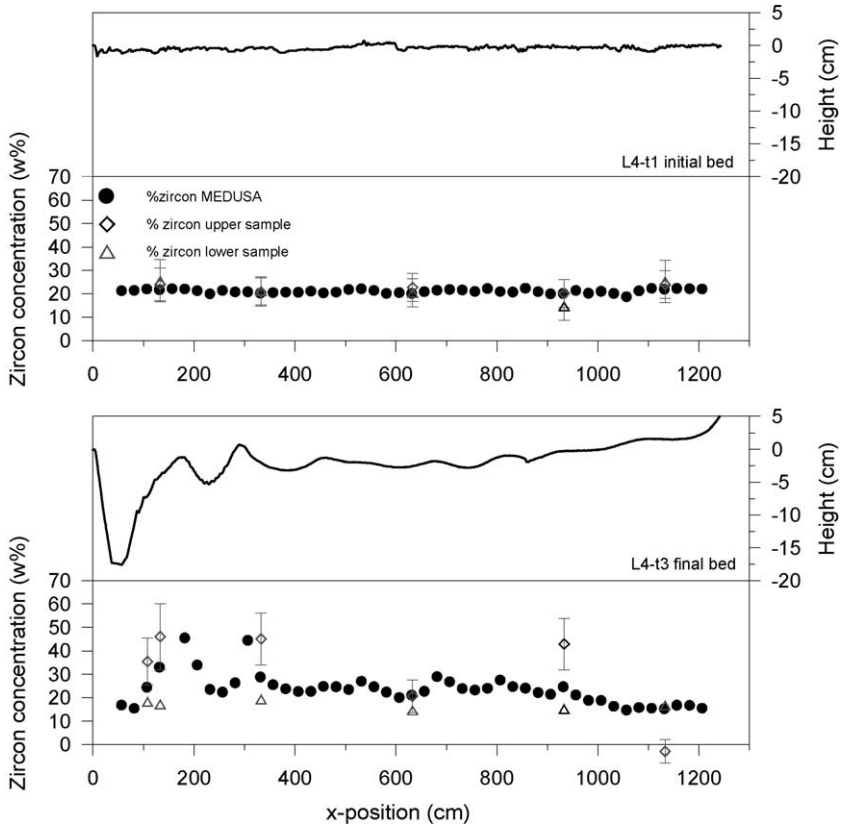

Fig. 4.3. Bed height, zircon concentration measured with MEDUSA (uncertainties fall within the data points) and zircon concentration measured from samples from the active layer and the immobile bed along the flume of the initial profile of condition L4 and the profile after three runs of condition L4.

shows an increased zircon concentration on the left-hand side of the flume, especially near the erosion hole, whereas at the right-hand side, downstream of about 10 m, the zircon concentration start to diminish from ~ 30% to 15%. In the syringe samples a clear difference of concentration with depth is observed. Within the uncertainties, the lower samples contain the zircon concentration of the initial bed, whereas for $x < 10$ m, the upper (typically 1–2 cm) an increased concentration is observed. For the far downstream sample ($x = 11.33$ m) the top slice of the syringe sample does not contain any zircons. In summary it can be concluded that the variations along the profile as measured with MEDUSA, originate from changes in the concentration in an active layer of 1–2 cm.

It should be noted that the zircon concentrations reflect changes in density (Eq. (2.7)). In the following, the measured zircon concentrations have been converted to densities.

4.1.2.2. Net-transport rates. Net-transport rates have been derived for the middle of the flume. They are based on the changes in volume and density in each section of the flume and the masses in the sand traps, corrected for loss of material (see Manso et al., 1999). In the L-series, no differences in the transport rates between left and right-hand side estimates were observed.

Fig. 4.4 shows the net total-transport rates as function of u_{rms}. The values of the transport rates for the density-mixed conditions (L3, L4 and L5) are larger than the values obtained by Ribberink and Al-Salem (1991) for uniform quartz sand. For conditions L1 and L2, sheet-flow conditions were not reached. However,

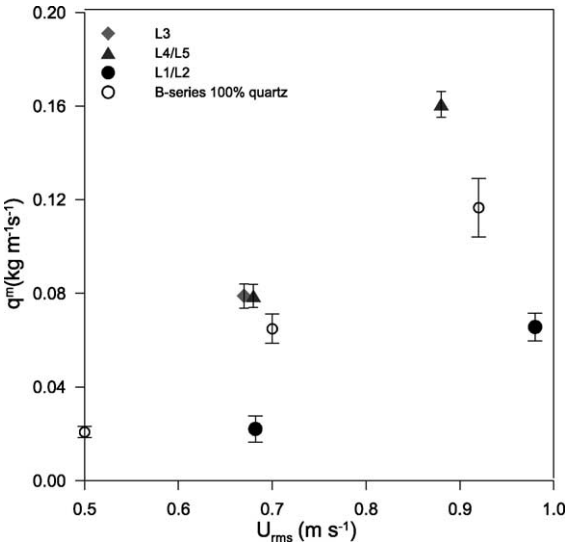

Fig. 4.4. Total transport rates for the L-series conditions and for some conditions of the B-series with uniform quartz sediments.

these results are shown to estimate the transport rates of pure zircon. If one compares the transport rates of pure zircon (L1 and L2) with L3, L4 and L5, one notices that the transport rates of L1 and L2 are considerably lower. L3 and L4 have similar hydrodynamic conditions, but differ in zircon content (7% and 25%, respectively). The higher zircon concentration in L4 is not reflected in the total transport rates.

4.2. Transport per fraction

From a modelling point of view, a size fraction method is often used in order to account for variations in sediment composition. In this approach, the sediment composition is divided in a number of fractions (i) with a frequency at the bed β_i. The transport rates are calculated for each fraction separately. The total transport rates are then calculated as:

$$q^{\mathrm{m}} = \sum_i \beta_i q_i^* . \tag{4.1}$$

The transport of the several fractions is assumed to be uncorrelated and q_i^* is the transport rate calculated as if the bed were composed of uniform material of fraction i. To account for non-uniformity effects, i.e. the sheltering of the smaller sizes in the lee of the larger sizes and the increased exposure of the larger grains, a correction factor is often applied to either the critical dimensionless shear stress or the effective bed shear stress in the computation of q_i^*.

In the comparison with previous experiments, not only the transport rates of the mixture will be compared with the transport rates of the well sorted sediment with equal grain size, but also the transport rates of the various fractions will be compared to the transport rates of the uniform sediment with equal properties and the frequency at the bed.

4.2.1. Size gradation

As mentioned in Section 2, Eq. (3.6) can be used to assess the sediment-transport rates per fraction in the central portion of the tunnel based on the mass of the fraction in the right-hand sand trap or in the left-hand sand trap. To solve this equation the sediment fractions μ_j^*, associated with the time-variations in the active layer, must be determined. In case of erosion, the sediment fractions μ_j^* are assumed to be equal to the fractions in the active layer μ_{Aj} as measured from sediment samples. The samples were taken at five locations along the tunnel of the initial bed. In case of sedimentation we assume that the sediment fractions μ_j^* are represented by the average of the fractions $\mu_{\mathrm{A}j}$ measured before and after the run. In principle, the active-layer thickness follows from Eq. (3.6) by considering the complete length of the tunnel. Subsequently, the transport rates per fraction follow from using Eq. (3.6) using the volumes in the left or, equivalently, right-hand side estimate. In practice, however, in some cases unrealistic (negative) values for the layer thickness were obtained. Cloin (1998) showed that the present measuring technique was not accurate enough to determine the active-layer thickness with sufficient accuracy. The uncertainty in the net-transport rates per fraction resulting from these uncertainties was assessed by a sensitivity analysis (Cloin, 1998) in which the net-transport rates per fraction were computed using a realistic range of active-layer composition and thickness. In Table 4.3 the transport rates for both the coarse and the fine fraction are given as well as the uncertainty, defined as the maximum of the standard deviation of either the transport rate per fraction over all runs per condition, or the standard deviation of the transport rate per fraction for the assumed range of active-layer composition and thickness. The results in Table 4.3 show

Table 4.3
Net transport rates per fraction (10^{-6} m^2 s^{-1})

Run	$\langle q_{avg} \rangle_{coarse}$	$\langle q_{avg} \rangle_{fine}$
K1	37 (8)	− 2 (8)
K2	13.1 (1.1)	3.9 (1.0)
K3	11.5 (1.6)	7 (2)
K5	52 (8)	27 (2)
K6	49 (9)	26 (9)

The estimated uncertainty (1 STD) is presented in brackets.

that in general the transport rates for the coarse fraction are considerably and significantly larger than for the fine fraction. We will return to these results in Section 5.

4.2.1.1. Conditions K5 and K6: sinusoidal waves plus current. In Eq. (4.1), the transport rate of a mixture is the sum to the product of the transport rate of the pure fraction times the abundance of the fraction. Fig. 4.5 shows for the conditions K5 and K6 the transport rates of the pure fractions (left) and the transport of the total mix and transport per fraction (right). For K5 one notices that the transport rate of the fine fraction is 50 ± 12% of the uniform fine sediment and the coarse fraction is 65 ± 10% of the uniform coarse fraction. This result is within the uncertainties in agreement with the transport rates that would have been derived with the size-fraction method Eq. (4.1). The sediment-transport rate of the medium sediment is equal to the transport rate of the mixture with similar median grain size.

For K6, the situation is different. Here, the relative transports per fraction are 37 ± 13% and 110 ± 20% for the fine and coarse fraction. Here the total transport rate corresponds again to the value of the uniform medium sediment. These results indicate that although the total transport rates of K5 and K6 is the same as the uniform sediment, considerable differences occur in the transport per fraction. Whilst in K5, the transport rates of coarse and fine material are determined by the availability in the bed, in K6 the transport rates of the coarse fraction is not limited by the availability whereas the fine fraction is reduced proportional to the availability.

4.2.1.2. Conditions K1 and K2: second-order stokes waves in the absence of a current. The transport rates for the uniform cases are determined from interpolation based on the third-power velocity-moment diagram in Fig. 4.2. Fig. 4.6 shows the total transport rates for uniform fine and medium sediments and the sediment-transport rates for the mixture as well as of the individual fractions. Although measurements on the uniform coarse fraction are not

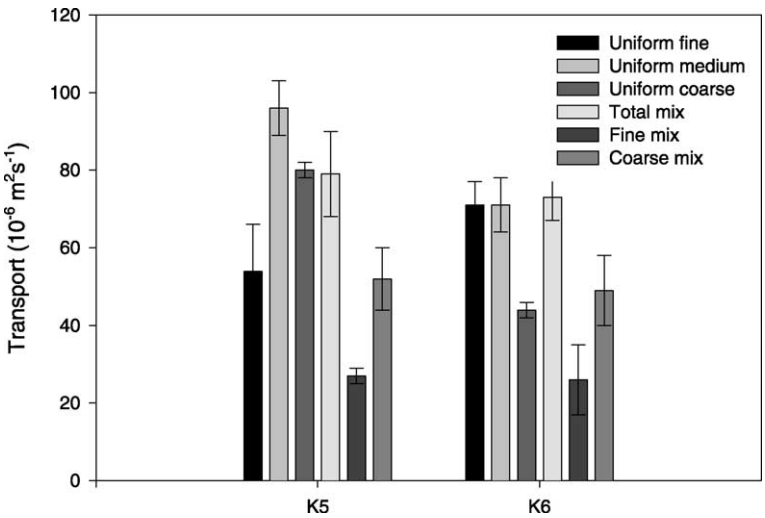

Fig. 4.5. Total net-transport rates in the middle of the flume for conditions K5 and K6, for uniform fine, medium and coarse sand based on interpolation and for the mixture total and fine and coarse fraction based on layer model.

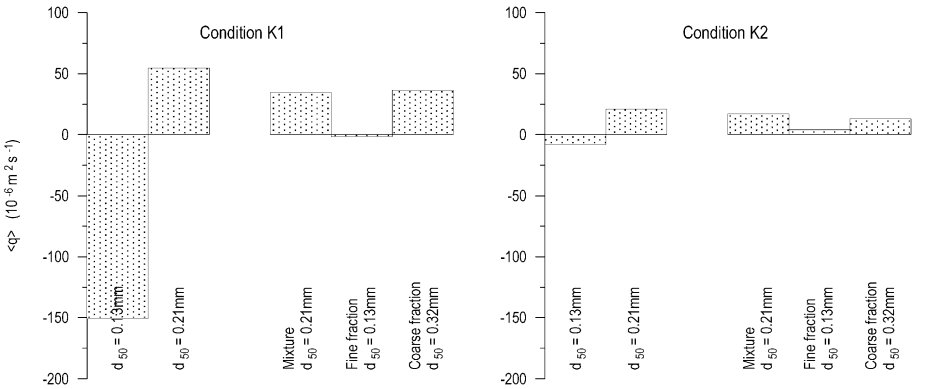

Fig. 4.6. Total net-transport rates for the middle of the flume conditions K1 and K2, for uniform fine and medium sand, based on interpolation, and for the mixture total, and its fine and coarse fraction based on layer model calculation.

available, we know that the ratios of the coarse fractions of K1 and K2 over the medium uniform fractions are 67% and 62%, respectively. Since we expect that the transport rates of the uniform coarse sediments are smaller than those of the medium-sized sediments, the ratio of the transport rate of the coarse fraction over the uniform coarse sediment would then be at least 67% and 62%, respectively. This would lead for condition K6 to the tentative conclusion that the coarse material is more easily transported than would be expected on basis of the availability at the bed.

For both K1 and K2, the transport rates of the mixture are dominated by transport rates of the coarse fraction. For condition K1 a non-significant transport of the fines in the mixture was found, compared to the large negative transport rates in the uniform fine sand. In K2 a small positive transport of fines is found in the mixture, whereas the uniform fine material is transported in opposite direction.

The fine fraction is reduced by the availability at the bed for sinusoidal waves plus a current, whilst the fines in the mixture show less effects of phase-lag in the second-order Stokes wave conditions. In most the experiments the transport rate of the coarse is larger than can be expected by their availability of the bed.

4.2.2. Density gradation

The transport rates for quartz and zircon have been derived from the analysis of the sand in the traps and the quantities entering Eq. (3.10). The results are presented in Fig. 4.7 for the net transport in the middle of the flume. The results in Fig. 4.7 indicate large differences between the transport of quartz and zircon.

A comparison of the transport rates of the quartz fraction with the sediment-transport rates of uniform quartz by Ribberink and Al-Salem (1992) (Fig. 4.7) gives ratios of 1.19 (0.10) for series L3, 0.94 (0.08) for L4 and 0.90 (0.07) for L5. This indicates that for all series, the transport rate of the lighter material is larger than can be expected on the availability at the bed. For the zircon, the ratios of the transport rates of the fractions with respect to the uniform material read 0.02 (0.02) for L3, 0.35 (0.11) for L4 and 0.59 (0.06) for L5. These results indicate that for the experiment with the low concentration of zircons (L3), the transport rate is lower than can be expected on the availability whilst the high energetic conditions of L5 point to an increased transport of zircon. However, we should point to the fact that the transport rates of uniform zircon were not under sheet-flow conditions.

4.3. Suspended sediment

4.3.1. General

In the K and L-series experiments, time-averaged suspended sediment concentrations $\langle C(z)\rangle$ were measured with a transverse suction concentration meter positioned at $x = 8.5$ m. The lowest suction tube was

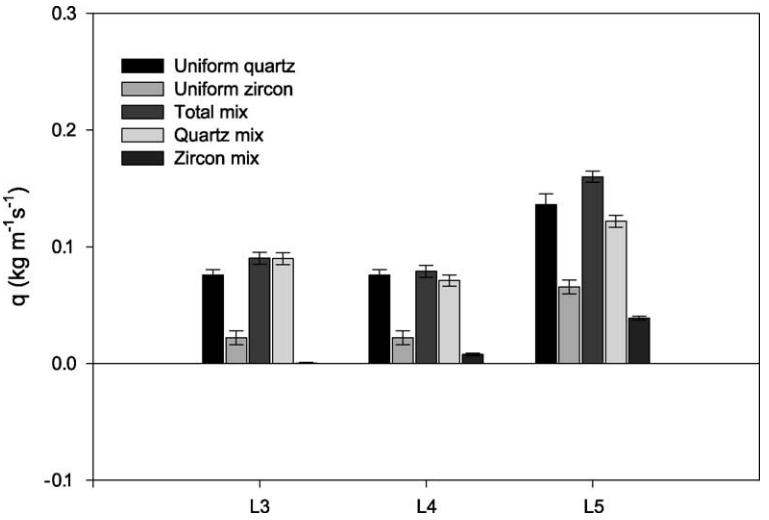

Fig. 4.7. Mass-transport rates for the quartz and zircon fraction compared with the uniform quartz measurements of Ribberink and Al-Salem (1991).

initially positioned at about 5 mm above the sediment, but the distance to bed changed during the experiments by an extra maximum 5 mm due to erosion at the bed.

Normally the suspended sediment is pumped into a bucket and after the experiment transferred to a volume meter. The amount of sediment collected is obtained by reading of the level in a volume meter after manually tapping on the tube. The conversion from volumes to masses is known for various grain sizes of quartz. Provided the density of the collected sediment is known, these conversion factors can be modified straightforwardly. In the K-series experiments only quartz was used and volumes were converted to masses. For the L-series, the volumes of most of the suspended sediments were too small to determine the density properly and hence only volumes are reported. However, settling velocities of samples of the lowest suction tubes (see Table 4.4) show that all values are consistent with the settling velocity of quartz, which indicates that only quartz minerals went into suspension.

Table 4.4
Settling velocities (in mm s^{-1}) at the lowest three tubes of the transverse suction system for the experiments L3, L4 and L5

Height above sediment (mm)	w_{s50}		
	L3	L4	L5
6	25	23	22
15	21	20	21
25		20	19

The measured values for quartz and zircon are 24 and 53 mm s^{-1}, respectively.

Time-averaged suspended-sediment concentrations are often described by a diffusion equation (Ribberink and Al Salem, 1994):

$$w_s\langle C\rangle + \varepsilon_s(z)\frac{d\langle C\rangle}{dz} = 0 \tag{4.2}$$

In this equation w_s represents the settling velocity and ε_s represents the sediment-mixing coefficient. By assuming that the sediment-mixing coefficient ε_s is constant in time and increases linearly with increasing distance z above the bed $a = z/\varepsilon$ (Al-Salem, 1993), the time-averaged concentration from Eq. (4.2) can be described by a negative-power distribution:

$$\langle C(z)\rangle = C_r\left(\frac{z}{r}\right)^{-\alpha} \tag{4.3}$$

with C_r being the reference concentration at $z = z_r$ ($z_r = 1$ mm in this case) and $\alpha = w_s a$, the concentration-decay parameter. As can been seen from Eq.

Table 4.5
Comparison of the concentration-decay parameter α for similar conditions

Condition	α	Condition	α	Condition	α
K2	1.25 (0.07)	K5	1.55 (0.03)	K6	1.23 (0.04)
C1	1.78 (0.08)	E2	2.20 (0.07)	E4	2.13 (0.06)
		H6	1.3	H9	1.4

(4.3), the mode of expressing the concentration, in either volume or mass per liter, is not relevant for the value of α as long as the density of the samples collected along the profile remains constant. The quantity α is a measure of the slope of the suspended-sediment profile: the larger α, the faster the suspended-sediment concentration decreases with increasing distance above the bed. Experiments by Ribberink and Al Salem (1994) showed that the α-parameter is constant for different u_{rms} velocities and the α-parameter depends only on the settling velocity.

During conditions K2 and K5 time-dependent concentrations were measured with a CCM in the sheet-flow layer and inside the bed. In the conditions K2, K5, K6, L3, L4 and L5 time-averaged sediment concentrations in the suspension layer were measured with the transverse suction system. In the following, only time-averaged concentrations will be presented both in the suspension layer (transverse suction) and the sheet-flow layer (CCM). The CCM concentrations were obtained by time-averaging the CCM signal.

4.3.2. Size gradation

4.3.2.1. Introduction. The sediment concentrations in the suspension and sheet-flow layers, measured during series K are compared with results of experiments with the same flow conditions but with uniform sands with $d_{50}=0.21$ mm and $d_{50}=0.13$ mm. In series K, condition K2 is compared with condition C1, condition K5 with condition E2 and H6 and condition K6 with condition E4 and H9 (for series references see Table 1.1). The comparison is considered as a first step to illustrate the gradation effects in sediment transport. For more details about the comparisons see also Katopodi et al. (1999).

4.3.2.2. Comparison of time-averaged concentrations in the suspension layer. The suspended-sediment samples of the K-series were also analysed on their median grain size in a settling tube. These analyses showed that the derived grain size decreases with increasing distance to the sediment bed, with a maximum $d_{50}=0.13$ mm at 5 mm above the sediment bed. This size is smaller than the d_{50} of the finest component of the bimodal distribution, and indicates that only the portion of the smaller grains of the finest fraction are primarily being suspended.

In series E the original sand with $d_{50}=0.21$ mm was suspended up to 2 cm. At elevations over 5 cm, the d_{50} drops to 0.18 mm. Stronger vertical sorting occurred in C1, where the d_{50} dropped to 0.13 mm for heights over 10 cm. This shows that even for uniform sand, selective sorting within the grain-size distribution occurs.

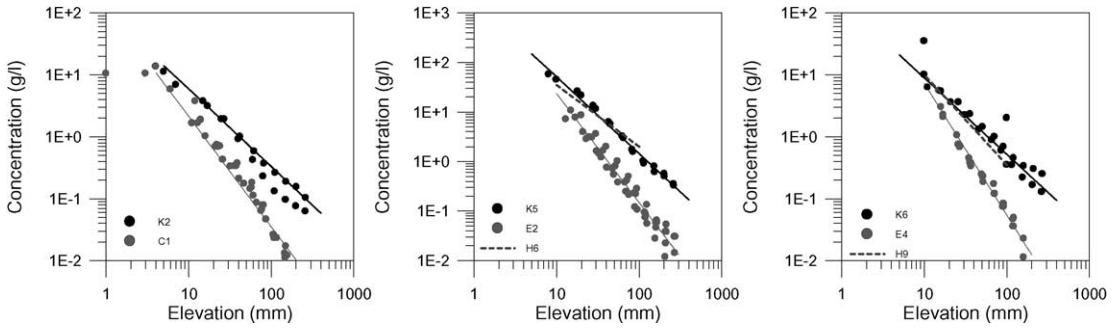

Fig. 4.8. Suspended-sediment concentrations, measured with the transverse suction system, as function of the height over the sediment bed for three combinations of conditions.

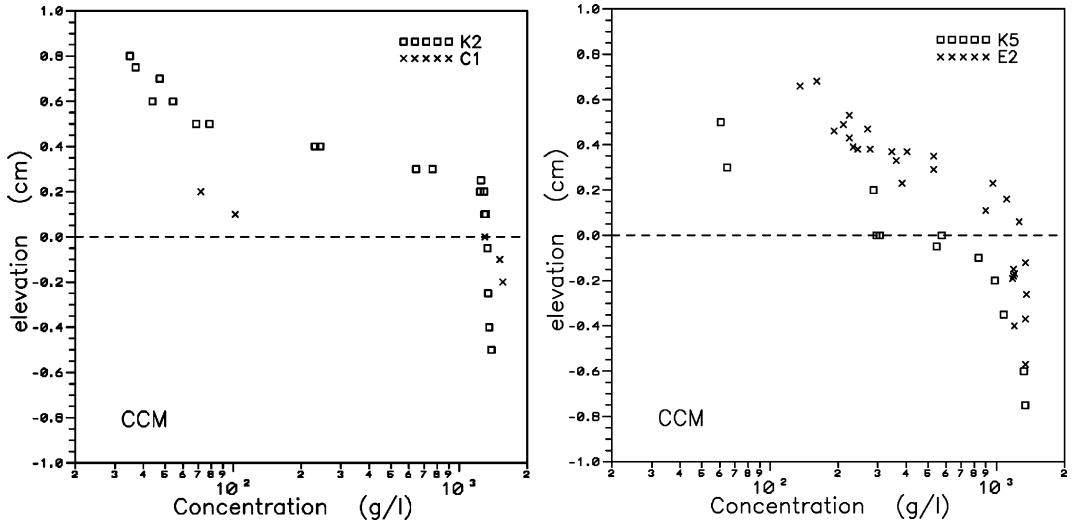

Fig. 4.9. Time-averaged concentrations measured with CCM for two pairs of conditions.

Eq. (4.3) is used to fit the suspended-sediment concentration profile of the K-series. Each run is fitted separately and the average value of the concentration-decay parameter α, for each series is calculated by taking into account the external uncertainty in α accounting for the correctness of the fit by a χ^2 method (Table 4.5).

Ribberink and Al Salem (1994) found that the value of the concentration-decay parameter for uniform sediment ($d_{50}=0.21$ mm) is almost constant ($\alpha=2.1$) in the velocity range of $u_{\mathrm{rms}}=0.3-0.9$ m s^{-1} under various wave conditions.

In Fig. 4.8 the time-averaged suspended-sediment concentration profiles measured with transverse suction are shown for the three pairs of conditions. For K5 and K6 the suspended-transport concentrations and the slope α (see Table 4.5) agree very well to those obtained in conditions H6 and H9 ($d_{50}=0.13$ mm) and differ considerably in magnitude and slope of the uniform $d_{50}=0.21$ mm data. This corroborates

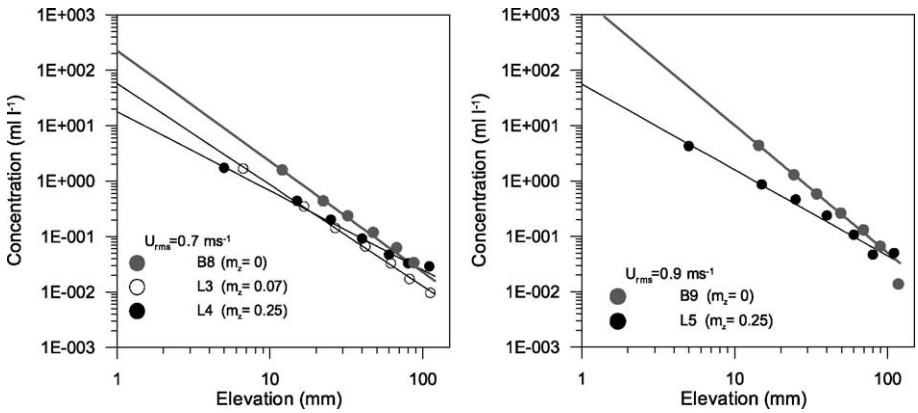

Fig. 4.10. Suspended-sediment concentrations over elevation.

the observation that smaller grain sizes in the distribution go into suspension. The similarity in magnitude points that the suspended transport is not limited by the availability at the bed. The shape and magnitude of the K2 series compared to the C1 data points to similar conclusions.

4.3.2.3. Comparison of time-averaged concentrations in the sheet flow layer. The time-dependent sediment concentration in the sheet-flow layer and below the bed was measured with a conductivity-concentration meter (CCM). The wave-averaged concentration was obtained by averaging the CCM signal over a number of wave cycles (Fig. 4.9).

These results differ from the comparisons of total transport rates. The total transport rates of K2 are smaller than C1, whilst the concentration in the sheet-flow layer show a reversed pattern, but the scarce data of the C1 experiment makes a firmer conclusion impossible. For the K5 experiment the comparison with E2 reveals a different pattern. Here the concentrations with the uniform sand (E2) are considerably higher than for the sand mixture (K5) for the same position over or in the bed, whilst the total transport rates are similar for both experiments.

4.3.3. Density gradation

Since the suspended sediments in the L-series experiments are only composed of quartz, it is expected that the α-parameter is constant for the different experiments and are comparable to the experiments with pure quartz.

Fig. 4.10 shows the suspended-sediment concentrations as function of elevation and the fits of Eq. (4.3). These results show, that opposite to the expectations, the slope of the suspension verticals changes with zircon concentrations in the bed and that the α-parameters decrease with increased concentration of zircon in the bed material (Table 4.6).

Table 4.6
α-Parameters for two u_{rms} velocities and varying zircon concentration of the sediment

Zircon concentration	α-parameter	
	0.7 m s^{-1}	0.9 m s^{-1}
0.25	1.43 (0.05)	1.55 (0.09)
0.07	1.83 (0.03)	
0	2.00 (0.04)	2.30 (0.01)

For the L-series experiments, all the α-parameters that describe the lower part of the suspended-sediment profile are smaller than 2.1 as reported by Ribberink and Al-Salem. The α-parameter for the experiment with 7% of zircon (L3) is larger than the α-parameter for both experiments with 25% of zircon (L4 and L5). Conditions L4 and L5 have the same α-parameter. A decreasing value of α for a constant settling velocity corresponds to an increased sediment diffusivity ε. According to Dohmen-Janssen (1999) an increased diffusivity corresponds to a thinner sheet-flow layer. In the L-series, the α-parameters are smaller than with pure quartz and decreases with increasing zircon concentration of the bed. Combining this information leads to the conclusion that the thickness of the sheet-flow layer decreases with increasing zircon concentration. This may explain why in the pure zircon experiments, sheet-flow could not be reached (Koomans, 2000).

5. Assessment and conclusions

The scope of this paper was to examine the effects of grain size and density gradation on sediment transport. Moreover we aimed at presenting a mathematical description that could serve as a basis to compute transport rates per sediment fraction.

5.1. Experimental techniques

The grain-size gradation experiments (series K) were conducted according to the measuring techniques and analysis methods proven to be successful in previous experiments with the LOWT: sediment composition was measured with a siphoning system in a thin layer (several centimetres) close to the sediment surface. In the density-gradation experiments (series L) a different approach was used: the differences in density required measurement techniques that could monitor the changes in density in the sediment bed along the flume. Therefore, measurements of natural radioactivity are used.

The validity of the volumetric approach in the K-series, especially with regard to the assumption that porosity was constant was investigated by applying a

mass-conservation equation to the total system, i.e. the entire flume and the two sand traps. The changes in porosity for all the three runs of L3 are consistent with zero. For the K-series experiments the values are statistically significant different from zero, and have a negative value. A negative value means a reduction in porosity, opposite to an expected increase due to segregation of the mixture into its components (see Section 1.2.2.1). Most likely effects of compaction dominate in the K2 series. The fact that these effects show up in the K-series and not in series-L is consistent with the procedure in which the erosion hole was filled after each run; in the series-L the erosion hole was allowed to develop during the entire experiment. In most of the runs of series K indicate that only small decreases ($\Delta\varepsilon \sim -0.001$) in porosity occur. In view of other systematic uncertainties, the compaction/segregation effects are ignored in the analysed data series. The results indicate that effects of change in bed structure due to the mixing and unmixing of the mixture is not of significant influence.

In the L-series, the sediment composition of the upper 8 cm of the sediment bed was determined with the MEDUSA system with a high spatial resolution along the tunnel. With these data, sediment transport per fraction could be calculated without the estimation of an active layer thickness.

5.2. Assessment of the formulations used in the measurements

The two series of experiments had a different nature of the sediment mixtures. As a result of the nature of the sediments used and the limitations of the available equipment and techniques for the different researches different procedures and different formulations were used. For the series K sediment composition could only been measured in a, thin, active layer. Therefore a modelling schematisation (active layer) had to be assumed, which added inaccuracies. In future work, an alternative procedure could be to extract entire columns (cores) of bed material for a direct and more accurate evaluation of the amount of solids per class $\rho\mu_f(1-\varepsilon_o)$.

The radiometric measurements with the MEDUSA system in series L gave information on the average composition of the total sediment column. Therefore, in the analysis of these experiments, assumptions on an active layer thickness were not necessary.

5.3. Total sediment transport

Previous work on experiments with different uniform grain sizes, showed that the increase in transport rates of fine sands was reduced with increasing $\langle u^3 \rangle$ by phase-lag effects (see e.g. Dohmen-Janssen, 1999). Whether these effects are still of importance when the fine sands are part of a mixture depends on the flow conditions of the experiment.

For the experiments of sinusoidal waves plus a current, the total transport rates of the uniform sediment are not significantly different from the transport rates of the total mixture with equal median grain size. For the condition with highest third-power velocity moment (small current, large waves), the transport rates of both fractions are limited by the availability at the bed. For the conditions with the lower third-power velocity (large current, small waves) moment, the transport rates of the fine fraction are determined by the availability at the bed, but transport rates of the coarse fraction are equal to the transport rate of the uniform coarse sediment. Here the bed availability is not limiting the transport rates.

In the experiments with a second-order Stokes wave, comparative measurements of the coarse fraction are not available, but an estimation based on the transport of the median grain size shows that the transport of the coarse fraction is at least equal or larger than half the transport rate of the uniform coarse. The comparison with the transport rates of the finest fraction and the transport rates of uniform fines shows that the mixed sediment transport rates are considerably lower than for the uniform case. A comparison of the total transport rates with transport rate of uniform sediment with equal grain size shows that the total transport of the mixture is smaller than in the uniform case. In a prediction of sediment-transport rates based on one d_{50}, were grading is not accounted for, the transport rates for the experiments with second-order Stokes waves would have been overestimated by a factor of 1.2–1.6. For all experiments it appears that the transport of the coarse fraction is larger than can be expected on basis of transport rates of uniform coarse sediment and the availability at the bed.

For the density-graded sediments, the total transport rates of the mixture are larger than the sediment-transport rates of pure quartz sediments. This is caused by the fact that the transport rates of the quartz fraction are not limited by the reduced availability at the bed, whilst the transport rates of zircons are equal to or higher than the transport rates that can be expected from the size-fraction method and the availability at the bed.

5.4. Suspended-sediment transport

The results on suspended-sediment transport of the size-graded sediments revealed that only the finest fraction is suspended and the concentration of the finest fraction is equal to the concentration of the uniform sediment with equal grain size. Therefore, the suspended-sediment concentrations are not hindered by the availability at the bed. This is surprising since for the experiments of sinusoidal waves plus a current, the net-transport rates show that the transport of fine material is reduced by the bed availability, but can be explained by realising that the suspended-sediment transport only accounts for 10–20% of the total transport. Since the suspended transport of fines in the sediment mixture is equal to the suspended transport of uniform fine sand, this indicates that effects of sediment grading on total sediment transport occur mainly in the bed-load transport in the sheet-flow layer.

For the density-graded experiments, it appeared that only the quartz minerals are suspended. This would indicate that the concentration-decay parameter, α, would be a constant. However, the results showed that this is not the case. This α-parameter decreases with increasing zircon concentration and point to an increased sediment diffusivity just above the sheet-flow layer with increased zircon concentration. Dohmen-Janssen (1999) attributes an increased sediment diffusivity to a decreased thickness of the sheet-flow layer.

5.5. Conclusion

In summary it can be concluded that gradation effects on sediment-transport rates can not been predicted by the transport rates of uniform sediment with equal grain size and the availability at the bed (size fraction method). The effects of size gradation are mainly in the increased transport rates of the coarse fraction with respect to the uniform coarse material and the availability at the bed under similar conditions. For conditions with sinusoidal waves plus a current, both sediment fractions behave as can be expected from the size-fraction method for the conditions with the smallest current, but for conditions with higher current, the transport rates of the coarse fraction is larger than can be expected on the availability at the bed and results from experiments with uniform material. The experiments on density-graded sediments indicate that total transport rates are larger than the transport rates of quartz material, whilst the transport rates of the quartz fraction show that this fraction is not hindered by the availability at the bed. The increase in zircon concentration at the bed causes and increase of the sediment-mixing coefficient just above the sheet-flow layer.

The mathematical description of the transport of graded sediment is derived in this work and shows that with improved techniques on the determination of the bed composition, assumptions on an active layer are not necessary for a correct description of the transport rates per sediment fraction, not only for experiments with heavy minerals, but also for grain-size gradation experiments. As has been shown in this paper the choice of quartz sand can be made such that a large enough difference in radiometric fingerprint is obtained. In that way a non-invasive measurement of the bed composition can be made.

We are convinced that this type of work needs further extension in experimental and theoretical direction. This work shows a clear need for further instrumental development. Porosity changes could play an important role, however, no direct porosity measurement technique is available. A possible way could be to measure porosity through bulk density by e.g. absorption of mono-energetic γ-rays. Such a measurement will yield an ε-value averaged over the volume between source and detector.

Acknowledgements

This work is carried out under the EU programme Marine Science and Technology III under contract

MAST3-CT95-0004. The experiments in the wave tunnel were part of the project of WL/DELFTHYDRAULICS in the framework of the EU programme "Training and Mobility of Researchers", contract ERBFMGECT950045. One of us (FM) is supported by the CICYT project #MAR97-0626 and Pedro Barrié de la Maza Foundation (Spain). The work is also part of the KVI research programme "Nuclear Geophysics".

References

Al-Salem, A.A., 1993. Sediment transport in oscillatory boundary layers under sheet-flow conditions, PhD Thesis, Technical University of Delft. 209 pp.

Andrews, E.D., 1983. Entrainment of gravel from naturally sorted riverbed material. Geological Society of America Bulletin 94, 1225–1231.

Armanini, A., Di Silvio, G., 1988. A one-dimensional model for the transport of a sediment mixture in non-equilibrium conditions. Journal of Hydraulic Research 26 (3), 275–292.

Armanini, A., Ruol, P., 1998. Non-uniform suspended sediments under waves. Proc. XXI ICCE, Malaga, Spain, 1129–1139.

Boon, J.D., Green, M.O., 1998. Caribean beach-face slopes and beach equilibrium. 21st ICCE, Malaga, Spain, pp. 1618–1630.

Bosman, J.J., van der Velden, E.T.J.M., Hulsbergen, C.H., 1987. Sediment concentration measurement by transverse suction. Coastal Engineering 11, 353–370.

Carling, P.A., 1983. Threshold of coarse sediment transport in broad and narrow natural streams. Earth Surface and Processes 8, 1–18.

Cheng, N.S., 1997. Simplified settling velocity formula for sediment particles. Journal of Hydraulic Engineering 123 (2), 149–152.

Cloin, B., 1998. Gradation effects on sediment transport in oscillatory sheet flow. WL/Delft Hydraulics report no. H2305, Delft.

Deigaard, R., Fredsoe, J., 1978. Longitudinal grain sorting by current in alluvial streams. Nordic Hydrology 9, 7–16.

de Meijer, R.J., 1998. Heavy minerals: from 'Edelstein' to Einstein. Journal of Geochemical Exploration 62 (1–3), 81–103.

de Moor, R.J., de Decker, R.J., 1982. Sedimentkenmerken van strandzanden op de Belgische kust. Natuurwetenschappelijk Tijdschrift 63, 49–80.

Dibanja, M., Watanabe, A., 1996. A transport-rate formula for mixed size sands. Int. Conf. on Coastal Engineering. ASCE, Orlando, USA.

Di Silvio, G., 1991. Sediment Exchange Between Stream and Bottom: A Four Layer Model Proc. Grain Sorting Seminar, Ascona, Switzerland, October, pp. 163–191.

Di Silvio, G., Peviani, M., 1991. Transport of a mixture of sand and gravel in suspension and as bed load: experiments and mathematical modelling. Proc. Int. Symposium on The Transport of Suspended Sediments and its Mathematical Modelling, Florence, pp. 623–638.

Dohmen-Janssen, M., 1999. Grain size influence on sediment transport in oscillatory sheet-flow. PhD thesis, Technical University, Delft, ISBN 90-9012929-4.

Egiazaroff, I.V., 1965. Calculation of non-uniform sediment concentrations. Journal of the Hydraulics Division, ASCE 91 (HY 4).

Eitner, V., 1995. Magnetic heavy mineral associations as sediment transport indicators on a beach of Norderney Island, Southern North Sea. Senckenbergiana Maritima 25 (4/6), 173–185.

Frihy, O.E., Komar, P.D., 1991. Patterns of beach-sand sorting and shoreline erosion on the Nile-Delta. Journal of Sedimentary Petrology 61, 544–550.

Frihy, O.E., Komar, P.D., 1993. Long-term shoreline changes and the concentration of heavy minerals in beach sands of the Nile Delta, Egypt. Marine Geology 115, 253–261.

Frihy, O.E., Lofty, M.F., Komar, P.D., 1995. Spatial variations in heavy minerals and patterns of sediment sorting along the Nile Delta, Egypt. Sedimentary Geology 97, 33–41.

Graton, L.C., Fraser, H.J., 1935. Systematic packing of spheres with particular relation to porosity and permeability. The Journal of Geology XLIII. Supplementary issue, November–December, pp. 785–909.

Greenfield, M.B., de Meijer, R.J., Put, L.W., Wiersma, J., Donoghue, J.F., 1989. Monotoring beach sand transport by use of radiogenic heavy minerals. Nuclear Geophysics 3, 231–244.

Guillén, J., Hoekstra, P., 1996. The "equilibrium" distribution of grain size fractions and its implications for cross-shore sediment transport: a conceptual model. Marine Geology 135, 15–33.

Hamm, L., Katopodi, I., Dohmen-Janssen, M., Ribberink, J.S., Samothrakis, P., Cloin, B., Savioli, J.C., Chatelus, Y., Bosboom, J., Nicholson, J., Hein, R., 1998. Grain size, Gradation and density effects on sediment Transport Processes in Oscillatory flow conditions, Part I: Gradation effects (series K), Data Report.

Hammond, F.D.C., Heathershaw, A.D., Langhorne, D.N., 1984. A comparison between Shields' threshold criterion and the movement of loosely packed gravel in a tidal channel. Sedimentology 31, 51–62.

Hirano, M., 1971. River bed degradation with armouring. Transactions on JSCE 3 (Part 2).

Horikawa, K., Watanabe, A., Katori, S., 1982. Sediment transport under sheet-flow condition. Proceedings of the 18th International Conference of Coastal Engineering, pp. 1335–1352.

Janssen, C.M., Ribberink, J.S., 1996. Grain size influence on sand transport in oscillatory sheet flow. 25th ICCE, Orlando, USA.

Janssen, C.M., Van der Hout, G., 1997. Sediment transport for two sands with different grain diameter under combined wave-current sheet-flow conditions, Data Report Z2137, Part I, Delft Hydraulics, The Netherlands.

Janssen, C.M., Hassan, W.N., Van der Wal, R.J., Ribbernik, J.S., 1996. Net sand-transport rates and transport mechanisms of fine sand in combined wave-current sheet-flow conditions, Data Report H2462, Part IV, Delft Hydraulics, The Netherlands.

Katoh, K., Yanagishima, S., 1995. Changes of sand grain distribution in surf zone. Coastal Dynamics, Gdansk, Poland, 639–649.

Katopodi, I., Ribberink, J.S., Ruol, P., Koelewijn, H., Lodahl C., Longo, S., Crosato, A., Wallace, H., 1994. Intra-wave sediment transport in an oscillatory flow superimposed on a net current,

Data Report H1684, Part III, Delft Hydraulics, The Netherlands.

Katopodi, I., Ribberink, J.S., Hamm, L., Kitou, N., Samothrakis, P., Dohmen-Janssen, C.M., Savioli, J.C., 1999. Comparison of concentration measurements with well-sorted and bimodal sand. Coastal Sediments '99, ACSE, Long Island, NY.

Kitou, N., Katopodi, I., 1999. Sediment grain size and density gradation. Mathematical formulation and approximations used in the TMR experiment, Report SAFE/02/99, Democritus University of Thrace, Dept. of Civil Engineering, Greece.

Komar, P.D., 1987. Selective grain entrainment by a current from a bed of mixed sizes: a reanalysis. Journal of Sedimentary Petrology 57, 203–211.

Komar, P.D., Wang, C., 1984. Process of selective grain transport and the formation of placers on beaches. Journal of Geology 92, 637–655.

Koning, A., 1947. Sedimenten met een hoog gehalte aan zware mineralen op het strand van Vlieland. Natuurwetenschappelijk Tijdschrift 29, 197–202.

Koomans, R.L., 2000. Sand in motion. Effects of density and frame size, Ph-D. Thesis, University of Groningen, The Netherlands. ISBN 90-367-1338-2.

Koomans, R.L., Bosboom, J., de Meijer, R.J., Venema, L.B., 1999. Effects of density on cross-shore sediment transport. Coastal Sediments, Long Island, New York.

Li, M.Z., Komar, P.D., 1992. Longshore grain sorting and beach placer formation adjacent to the Columbia River. Journal of Sedimentary Petrology 62, 429–441.

Liu, J.T., Zarillo, G.A., 1987. Partitioning of shoreface sediment grain sizes. Coastal Sediments, New Orleans, USA, pp. 1533–1548.

Manso, F., Koomans, R.L., Groen, P.W.C., de Meijer, R.J., 1999. Grain size gradation and density effects on sediment transport processes in oscillatory flow conditions, Part II: The effects of density gradation (Series L), Data report.

May, J.P., 1973. Selective transport of heavy minerals by shoaling waves. Sedimentology 20, 203–211.

Meisburger, E.P., 1989. Cross shore variations in heavy minerals in beaches of the barrier dominated south-east Atlantic coast. Proceedings of Coastal Zone Conference '89, Charleston, pp. 93–105.

Migniot, C., Lorin, J., 1986. Study of suspended load concentration under the action of waves. La Houille Blanche 3, 211–219.

Moutzouris, C.I., 1988. Longshore sediment transport rate versus cross-shore distribution of sediment grain size. 21st ICCE, Malaga, Spain, pp. 1959–1973.

Peterson, C.D., Komai, P.D., Scheidegger, K.F., 1985. Distribution, geometry and origin of heavy mineral placer deposits on Oregon Beaches. Journal of Sedimentary Geology 56 (1), 67–77.

Pruszak, Z., 1993. The analysis of beach profile changes using Dean's method and empirical orthogonal functions. Coastal Engineering 19, 245–261.

Rahuel, J.L., Holly, F.M., Chollet, J.P., Bellendy, J.P., Yang, G., 1989. Modelling of riverbed evolution for bedload sediment mixtures. Journal of Hydraulic Engineering, ASCE 115 (11).

Ribberink, J.S., 1987a. Mathematical modelling of one-dimensional morphological changes in rivers with non-uniform sediment, PhD thesis, Delft University of Technology.

Ribberink, J.S., 1987b. Mathematical modelling of one-dimensional morphological changes in rivers with non-uniform sediment, Doc. Thesis, Civil Eng. Dep., Delft Univ. of Technology, Delft, The Netherlands.

Ribberink, J.S., 1989. The large oscillating water tunnel: technical specifications and performances. Technical report, Delft Hydraulics, Delft, The Netherlands.

Ribberink, J.S., Al-Salem, A., 1991. Sediment transport, sediment concentrations and bedforms in simulated asymmetric conditions. Delft Hydraulics Report H840, Part IV, The Netherlands.

Ribberink, J.S., Al-Salem, A.A., 1992. Bedforms, near-bed sediment concentrations and sediment transport in simulated regular waves. Delft Hydraulics report H-840.

Ribberink, J.S., Al Salem, A.A., 1994. Sediment transport in oscillatory boundary layers in cases of rippled beds and sheet flow. Journal of Geophysical Research 99 (C6), 12707–12727.

Ribberink, J.S., Chen, Z., 1993. Sediment transport of fine sand under asymmetric oscillatory flow, Report H840, Part VII, Delft Hydraulics, The Netherlands.

Richmond, B.M., Sallenger, A.H., 1984. Cross-shore transport of bimodal sands. 19th ICCE, Houston, USA, pp. 1997–2007.

Roelvink, J.A., Meijer, J.P.G., Houwman, K., Bakker, R., Spanhoff, R., 1995. Field validation and application of a coastal profile model. Proceedings Coastal Dynamics 1997, pp. 818–828.

Slingerland, R.L., 1984. Role of hydraulic sorting in the origin of fluvial placers. Journal of Sedimentary Petrology 54, 137–150.

Tánczos, I.C., 1996. Selective transport phenomena in coastal sands, PhD thesis University Groningen, ISBN 90-367-0669-6.

Tánczos, I.C., Janssen, M.C.M., Ribberink, J., de Meijer, R.J., November 1995. Selective transport study in a large wave tunnel (Data report), KVI-internal report, Z-33.

Terwindt, J.J., 1962. Study of grain size variations at the coast of Katwijk, The NetherlandsNote K-324, Rijkswaterstaat. Deltadienst, Den Haag.

Van der Hout, G., 1997. Grain size and gradation effects on sediment transport under sheet-flow conditions, Part 2: Data Analysis and modelling. Report Z2137, WL/Delft Hydraulics, Delft, The Netherlands.

Van der Wal, R.J., 1996. Grain-size influence on sediment transport in sheet-flow conditions in combined wave-current flow. MSc thesis, Delft University of Technology, The Netherlands, 104 pp.

Van Rijn, L.C., 1997a. Cross-shore sand transport and bed composition. Proceedings Coastal Dynamics, 88–98.

Van Rijn, L.C., 1997b. Cross-shore modelling of graded sediments, WL/Delft Hydraulics report Z2181.

Veenstra, H.J., Winkelmolen, A.M., 1976. Size, shape and density sorting around two barrier islands along the north coast of Holland. Geologie en Mijnbouw 55, 87–104.

Venema, L.B., De Meijer, R.J., 2001. Natural radionuclides as tracers of dispersal of dredge spoils dumped at sea. Journal of Environmental Radioactivity 55, 221–239.

von Engelhardt, W., 1937. Über die Schwermineralsande zwischen Warnemünde und Darsser Ort und ihre Bildung durch die Brandung. Zeitschrift fuer Angewandte Mineralogie 1 (1), 30–59.

Winkelmolen, A.M., Veenstra, H.J., 1980. The effect of a storm surge on near-shore sediments in the Ameland-Schiermonnikoog area, N. Netherlands. Geologie en Mijnbouw 59, 97–111.

Winterkorn, H.F., Fang, H.Y., 1975. Foundation Engineering Handbook Van Nostrand Rainhold, New York. 737 pp.

Yeganeh Bakhtiary, A., Asano, T., 1998. Effects of particle properties on oscillatory sheet-flow dynamics. Coastal Engineering Journal 40 (1), 61–80.

Zyserman, J.A., Fredsoe, J., 1991. Including the effect of graded sediments in a deterministic transport model. MAST-G6M Mid-Term Workshop, Edinburgh.